J. Ind. Geophys. Union (April 2016)
v.20, no.2, pp: 151-170

Site-specific Next Generation Ground Motion Prediction Models for Darjeeling-Sikkim Himalaya using Strong Motion Seismometry

Manik Das Adhikari and Sankar Kumar Nath*

Department of Geology & Geophysics, Indian Institute of Technology Kharagpur, West Bengal, Pin: 721302, India
*Corresponding Author: nath@gg.iitkgp.ernet.in

ABSTRACT

In the perspective of Probabilistic Seismic Hazard Assessment, the ground motion parameters at a site of interest are evaluated by using a ground motion prediction equation that relates a specific strong motion parameter of ground shaking to one or more seismic attributes. In this study, we deliver site-specific Next Generation Prediction (NGP) Models for Darjeeling-Sikkim terrain located in the eastern Himalayan seismogenic province implicating a maximum credible earthquake of magnitude M_w8.3. The NGP models have been developed for three dominant tectonic domains viz. normal, strike-slip and thrust faulting mechanism of earthquake nucleation as per site classes A, B, C & D for different station elevation ranges for Peak Ground Acceleration (PGA) and 5%-damped Pseudo Spectral Acceleration (PSA) at 0.2 and 1.0 sec time period as a function of magnitude, fault rupture distance and site condition. The Extended Finite Fault simulation approach EXSIM is used for ground motion synthesis with the source parameters extracted from the recorded and historical earthquakes reported in the territory. In order to strengthen the ground motion data base, the seismic events of small to moderate magnitude with signal-to-background noise ratio≥ 3 recorded by Darjeeling-Sikkim Strong Motion Array of IIT Kharagpur have been amalgamated with the simulated ones for a wide magnitude range of M_w3.5 to 8.3 at 140 locations at a grid spacing of $0.1^o \times 0.1^o$. Altogether 42 ground motion prediction equations have been worked out through a nonlinear regression process of strong ground motion data versus magnitude, distance, and other predictive variables using two classical ground motion attenuation models which predicted 14 coefficients for each of the derived equations depicting zero clustered residuals. The derived NGP models have been used in a logic tree framework for probabilistic seismic hazard assessment of the Darjeeling-Sikkim Himalaya depicting PGA distribution for 10% probability of exceedance in 50 years at surface level varying from 0.293g to 0.807g. The major urban centers viz. Gangtok, Mangan, Singtham, Melli, Jorethang, Uttare and Darjeeling are seen to have enhanced hazard level to the tune of 0.60 - 0.750g placing those to probable Seismic Zone V with the suggested zone factor of 0.75g.

Key words: Next Generation Prediction(NGP), Seismic Source Attributes, Strong Ground Motion Data, Generic Site Amplification, Darjeeling-Sikkim Himalaya.

INTRODUCTION

Darjeeling-Sikkim Himalaya located in the earthquake prone fold thrust belt of the Eastern Himalayas along Darjeeling-Sikkim tract is seismically active with the incidence of moderate to large magnitude earthquakes in the terrain. Seismic hazard and microzonation of densely populated urban centers necessitates adaptation of appropriate Ground Motion Prediction Equations (GMPE) that relates a specific ground motion in the form of Peak Ground Acceleration (PGA), Peak Ground Velocity (PGV), Pseudo Spectral Acceleration (PSA) and/or Peak Ground Displacement (PGD) to one or more earthquake parameters viz. source, the wave propagation path between the source and the site and the soil /engineering rock stratum or geological site condition. The prediction equations are developed by the statistical evaluation of a large set of ground motion data for different regions and tectonic types. Recent reviews on the development and application of ground motion attenuation models can be found in Douglas (2003), Power et al (2008) and Nath & Thingbaijam (2011).

We analyzed about 350 seismic events of magnitude ranging between M_w2.5 to M_w6.9 in Darjeeling-Sikkim Himalaya as recorded by the Darjeeling-Sikkim Strong Motion Network of IIT Kharagpur. Thingbaijam and Nath (2008) have predicted the maximum credible earthquake of M_w8.3 in the eastern Himalayas. In order to strengthen the ground motion data base covering a wide magnitude range of M_w3.5 to 8.3, strong ground motion synthesis is performed systematically. Starting with the empirical models of Boore & Atkinson (2008) and Campbell & Bozorgnia (2003), the Next Generation Prediction (NGP) models developed in the present study include PGA, PSA at different periods for three tectonic types viz. normal, strike-slip and thrust faulting mechanism responsible for triggering earthquakes in this terrain (Mishra 2014).

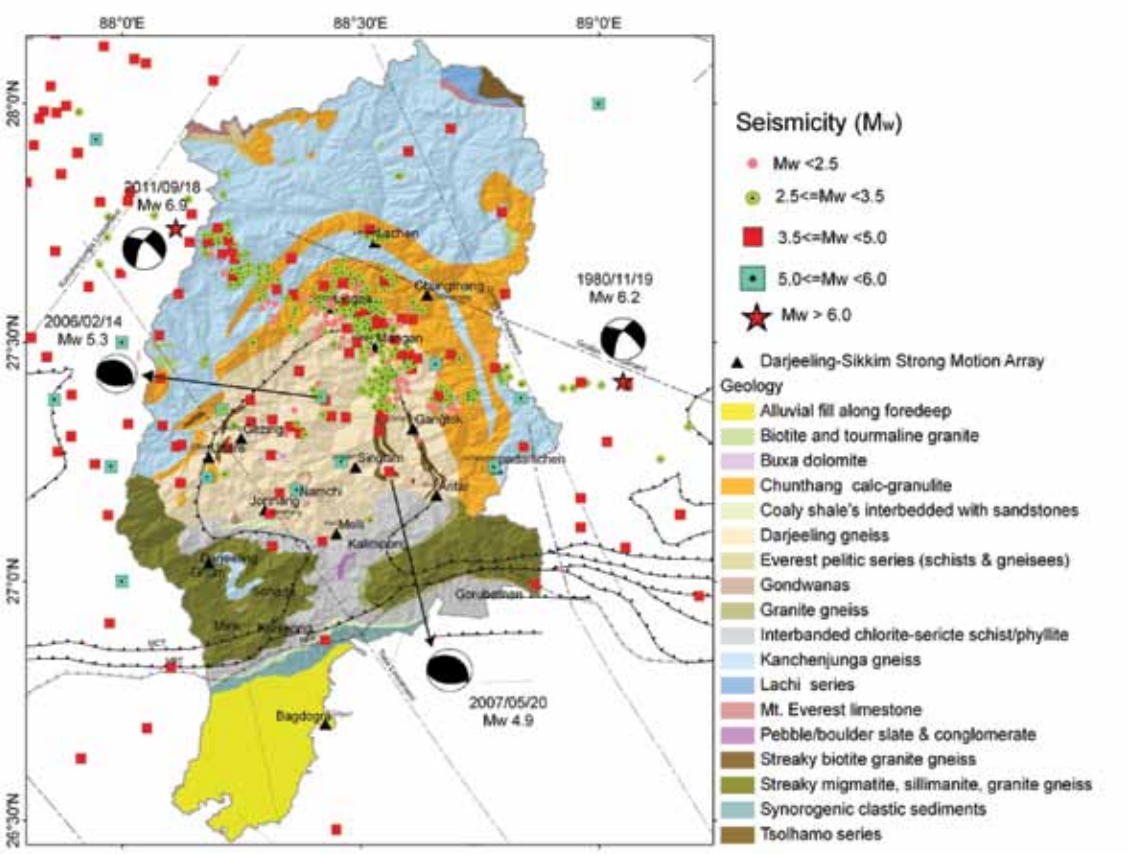

Figure 1. Seismotectonic Map (Modified after Dasgupta et al. 2000) depicting the Darjeeling-Sikkim Strong Motion Array and recorded earthquakes in Darjeeling-Sikkim Himalaya.

MATERIALS AND METHODS

Data:

One Kinemetrics Altus K2 and 13 Kinemetrics Altus ETNA strong motion accelerographs were installed by IIT Kharagpur at Gangtok, Mangan, Singtam, Melli, Chungthang, Lachen, Lingza, Padamchen, Aritar, Jorethang, Uttare, Gezing, Darjeeling and Siliguri as shown in Figure 1 to continuously monitor earthquakes in the earthquake prone Darjeeling-Sikkim Himalayan districts. The digital accelerographs 'ETNA' of Kinemetrics make are of high dynamic range of 108 dB @ 200 samples/sec and 18 bit resolution set at a trigger level of 0.02% of the full scale (2g). The Darjeeling-Sikkim Strong Motion Array (DSSMA) has been operative since 1998 recording more than 350 earthquakes till date as shown in Figure 1 with about 55 events of magnitude M_w<2.5, about 210 events with magnitude between M_w2.5 - 3.5, about 73 events with magnitude ranging from M_w3.5 - 5.0 and about 12 events with magnitude from M_w5.0 - 6.9. 30 representative well-located earthquakes with good signal-to-noise ratio (signal-to-background ratio ≥3) in the region for the period 1998-2012 have been presented in Table 1. These earthquakes have hypocenter depths ranging from 7.4 km to 70 km. Among these, December 2001 of M_L5.6, February 2006 of M_w5.3 and September 2011 of M_w6.9 caused wide spread damage in the region. However, Nath et al (2005), Pal et al (2008) and Nayak et al (2011) have used subset of these data for the estimation of seismic source parameters and also to work out the path attenuation model of the region.

Seismotectonism and seismic source attribution:

Darjeeling-Sikkim Himalaya has a series of longitudinal tectono-stratigraphic domains (Gansser 1964) such as 1) Sub-Himalayas, 2) Lesser Himalayas, 3) Higher Himalayas, and 4) Tethys Himalayas which are separated by major dislocation zones consisting of Main Boundary Thrust (MBT), Main Central Thrust (MCT), NNW-SSE trending Tista and Gangtok Lineaments, WNW-ESE trending Goalpara Lineament and SW-NE trending Kanchanjunga Lineament as depicted in the Geological Map of Figure 1. The Siwalik rocks in the Sikkim Himalaya rises from the alluvial plain with a tectonic demarcation by the Himalayan Frontal Thrust (HFT) which is termed as Main Frontal Thrust (MFT) in Nepal (Thakur et al. 2012). As proposed by Barazangi and Ni (1982) the Indian plate continues

Table 1. 30 representative earthquakes recorded by Darjeeling-Sikkim Strong Motion Array (DSSMA) with signal-to-background noise ratio≥ 3.

Sl.	Event (YYMMDDHHMM)	Latitude (°N)	Longitude (°E)	Magnitude	Depth (Km)
1	9903070614	27.25	88.39	4.8	23.58
2	0008071359	27.28	88.33	4.8	10
3	0006290426	27.4	88.83	4.8	10
4	0011172135	27.24	88.54	5	10
5	0006070910	27	88	5.1	18.98
6	0005310321	27.55	88.4	5.2	7.4
7	0007041026	27.17	88.45	5.3	24.52
8	0006160612	27.68	88.29	5.4	10
9	0010030502	27.23	88.48	5.5	34.27
10	0111160424	27.36	88.16	5	19.02
11	0111231031	27.37	88.43	5	10
12	0112022241	27.25	88.46	5.6	26.25
13	0208221612	27.135	88.388	5	16.48
14	0204291243	27.2	88.7	5.2	27.83
15	0204250116	27.15	88.83	5.3	10
16	0204250458	27.28	88.63	5.3	22.9
17	0204251130	27.32	88.3	5.3	26.4
18	0204300646	27.91	88.54	5.4	10
19	0205021028	27.97	88.7	5.5	10
20	0309291340	27.36	87.74	4.8	33
21	0402180123	27.36	87.76	4.9	20
22	0402271253	28.13	87.66	5	68
23	0506141423	27.2	87.92	4.8	44
24	0508281214	27.64	87.42	5	38
25	0602140625	27.35	88.35	5.3	30
26	0608111435	27.34	87.74	5.2	35
27	0708111435	27.5	88	5.5	33
28	1112142020	27.7	88	4.7	50
29	1109181157	27.45	88.39	4.8	16
30	1109181240	27.74	88.133	6.9	47.4

to subduct below the Tibetan Plateau up to South Lhasa facilitated by Main Himalayan Thrust (MHT), considered as the decollement plane. Incidentally Nakata et al (1990) reported neotectonic activity along HFT. Thus, the region possesses high seismic threat due to the tectonic fragmentation of Central Himalaya, Northeast India and Tibetan Plateau. Mishra (2014) reported that the seismicity located beneath the Darjeeling-Sikkim Himalaya showed mixed type of faulting i.e. thrust, strike-slip, and normal which indicate the intricate seismotectonic set-up and the existence of the transverse tectonic features while the seismicity beneath the Tibetan Plateau exhibits large component of normal and strike-slip faulting (Molnar and Chen 1983, De la Torre et al. 2007, Molnar and Lyon-Caent 1989).

A great earthquake of M_w8.1 struck eastern Nepal region, close to Darjeeling-Sikkim Himalaya, in January 1934 with its epicenter located in the Bihar-Nepal region (Sapkota et al. 2013) inducing ground motion equivalent to MM intensity VII in the region (GSI 1939). The 1897 Shillong earthquake occurred south of Sikkim in the Shillong Plateau region causing damage equivalent to MM intensity VI in the Darjeeling-Sikkim region. The 1950 Assam earthquake of M_w8.7, 1930 Dhubri earthquake of

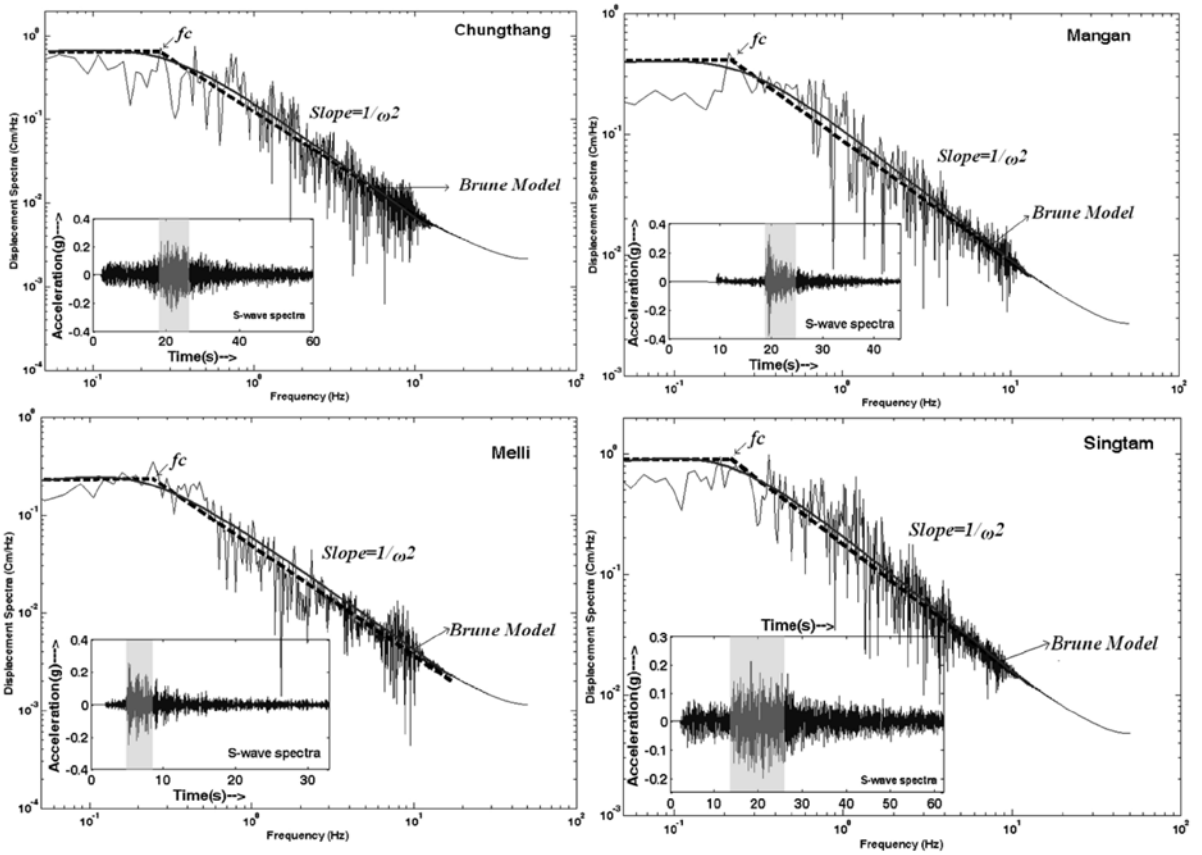

Figure 2. Representative S-wave Displacement Spectra of a few events recorded at Chungthang, Mangan, Melli and Singtam stations of Darjeeling-Sikkim Strong Motion Array of IIT Kharagpur.

M_w7.1 and 2009 Bhutan earthquake of M_w6.1 also caused wide spread damage in the territory. In the recent past Darjeeling-Sikkim experienced an M_w6.1 earthquake on 19th Nov 1980, an M_w5.3 earthquake on 14th February 2006 and more recently on 18th Sept 2011 an M_w6.9 event.

Source parameters from Fourier displacement spectra in terms of corner frequency (f_c), seismic moment (M_o), stress drop ($\Delta\sigma$) and average displacement (u) are calculated from the recorded waveform data. In the present study, the recorded acceleration data are double integrated after applying the instrument response and baseline corrections and filtered between 0.5 and 30 Hz using a Butterworth band-pass filter to determine the displacement. For estimating the spectral source parameters, we first chose a suitable time window around the S-wave arrival on the displacement seismogram as shown in Figure 2 for 2011 Sikkim earthquake of M_w6.9 recorded at Chungthang, Mangan, Melli and Singtam stations of DSSMA. The shear-wave phases (including direct, reflected, and refracted phases) are picked up using time windows of varying length depending on the record length with each window selected to include the strongest shaking (Nayak et al. 2011). We then fitted two lines to the displacement spectra; one horizontal component to define the long period spectral level Ω_o, at lower frequencies and the other at a gradient corresponding to the fall-off at higher frequencies as depicted in Figure 2 for S-wave spectra at all the seismic stations of which only four representatives are presented here. The intersection of the two lines determines the corner frequency (f_c) as indicated in the diagrams. Seismic moment 'M_o' for S-wave components of the spectra can be estimated from the relation:

$$M_o = \frac{4\pi\rho V_s^3 \Omega_0 R}{(kR^{\theta\phi})} \quad (1)$$

where, V_s is the S-wave velocity at the source assumed to be 3.8 km/sec (Nath et al. 2005, Raj et al. 2009, Acton et al. 2011), 'k' is the free surface operator assumed to be equal to '2' and $R^{\theta\varnothing}$, the radiation pattern considered to be equal to 0.55 following Raj et al. (2009), Ω_o is the low frequency level on the spectra, 'R' is the hypocentral distance, 'ρ' = 2.7 gm/cm^3 (Nath et al. 2005, Raj et al. 2009) is the density of the medium.

The source radii (r) have been computed using corner frequency f_c, for the Brune model (Brune 1970) considered for describing the earthquake source as,

$$(r_B) = 0.37\frac{V_s}{fc} \quad (2)$$

Stress drop ($\Delta\sigma$) has been estimated from seismic moments and source radii of the S-wave segment of the ground motion data from Brune (1968) as,

$$\Delta\sigma = 0.44\frac{M_0}{r^3} \quad (3)$$

The seismic moment estimated using the present data set ranges from 3.8×10^{21}-1.5×10^{25} dyne-cm. It is also observed that the corner frequency (f_c) varies between 0.22 – 1.35 Hz while the estimated stress drop using Brune model ranges between 0.75 to 147 bars. As reported in earlier studies on source parameters of earthquakes nucleated in Darjeeling-Sikkim Himalaya, by Sharma and Wason (1994), Singh et al (1978), Kumar et al (2005), Gupta and Singh (1980), Nath et al (2005), Chopra et al (2014) the Brune's model is considered to be more realistic and hence is adopted for strong ground motion synthesis in the present investigation.

Ground motion analysis and synthesis:

The quantitative assessment of seismic hazard necessitates measurement of a peak ground motion parameter, such as the PGA from earthquake records. Earthquakes occurring at large epicentral distances from a site can cause significant devastations, which are primarily associated with long-period components of the seismogram. The waveforms are also affected by the source directivity and path characteristics (Thingbaijam and Nath 2008). However, the influence from the former is considerably less at large epicentral distances. Paucity of good magnitude coverage of strong ground motion data, analytical or numerical approaches for a realistic prognosis of possible seismic effects in terms of tectonic regime, earthquake size, local geology, and near fault conditions requires systematic ground motion synthesis (Anbazhagan et al. 2013). There are several algorithms available for ground motion synthesis. However, finite-fault stochastic method is considered to be the best option due to its capability of handling larger fault rupture distances and also the source characteristics especially the near-field effect (Sengupta 2012). The approach given by Motazedian and Atkinson (2005) is based on the introduction of dynamic corner frequencie. The major feature of the technique is the conservation of the radiated energy at high frequency at any sampling of the sub-fault size such that the relative amplitude of higher versus lower frequencies is controlled (Nath et al. 2009, Sengupta 2012). The amplitude spectrum due to the i^{th} sub-fault can be written as;

$$A_i(f) = CM_{oi}H_i\frac{(2\pi f)^2}{1+(f/f_{oi})^2}\exp(-\pi f\kappa)\times\exp\left(-\frac{\pi f R_i}{\beta Q}\right)G \quad (4)$$

where, M_{0i} is the seismic moment of the i^{th} sub-fault, R_i is the sub-fault distance from the observation point, and G, β and Q are geometric attenuation, shear wave velocity, and quality factor, respectively. In the above equation, the κ filter given by Anderson and Hough (1984) defined as $\exp(-\pi f\kappa)$ is incorporated to achieve decay of the higher frequency spectra. The constant $C = R^{\theta\varphi}FV/(\rho\pi\beta^3)$ where $R^{\theta\varphi}$ is the radiation pattern (average value of 0.55 for shear waves), ρ is the density, and F is the free surface amplification (2.0) while V (= 0.71) is the partition between two horizontal components. The seismic moment (M_0) and stress drop ($\Delta\sigma$) can be related as;

$$f_{oi} = 4.9\times10^6\left(N_R(t)\right)^{-1/3}N^{1/3}\beta\left(\frac{\Delta\sigma}{M_0}\right)^{1/3} \quad (5)$$

where, $\Delta\sigma$ is the stress drop in bars, fc is in Hz, β in km/sec and M_0 in dyne-cm (Brune 1970). $N_R(t)$ is the total number of sub-faults ruptured at a time t, and the dynamic corner frequency for ith sub-fault is represented by f_{0i}. H_i is the scaling factor responsible for conserving energy at the high frequency spectral level of sub-faults, which is defined as;

$$H_i = \left(N\frac{\sum_f\left(\frac{f^2}{1+(f/f_o)^2}\right)^2}{\sum_f\left(\frac{f^2}{1+(f/f_{oi})^2}\right)^2}\right)^{1/2} \quad (6)$$

where, f_0 is the corner frequency at the end of the rupture, i.e., the corner frequency of the entire fault, with $N_R(t) = N$. Following Ordaz & Singh (1992) and Castro et al. (1996) the geometric function given in equation (7) has been considered to take into account the possible arrival of surface waves in the windowed data,

$$\begin{aligned} G(R) &= 1/R && \text{for } R<100\text{km} \\ &= (R*100)^{-0.5} && \text{for } R>100\text{km}. \end{aligned} \quad (7)$$

The simulation parameters considered in the present study are listed in Table 2. The width and length of the fault is calculated using the formulations of Well and Coppersmith (1994). Q_o is taken as 167 and eta is taken as 0.47 (Nath et al. 2008). Simulation is performed at 140 locations in the grid with a spacing of $0.1^o\times0.1^o$ using EXIM code developed by Motazedian and Atkinson (2005). The velocity model given by Action et al (2011) is used in the present investigation. The representative crustal model illustrated in Table 3 is employed for the first order estimation of crustal amplification based on quarter-

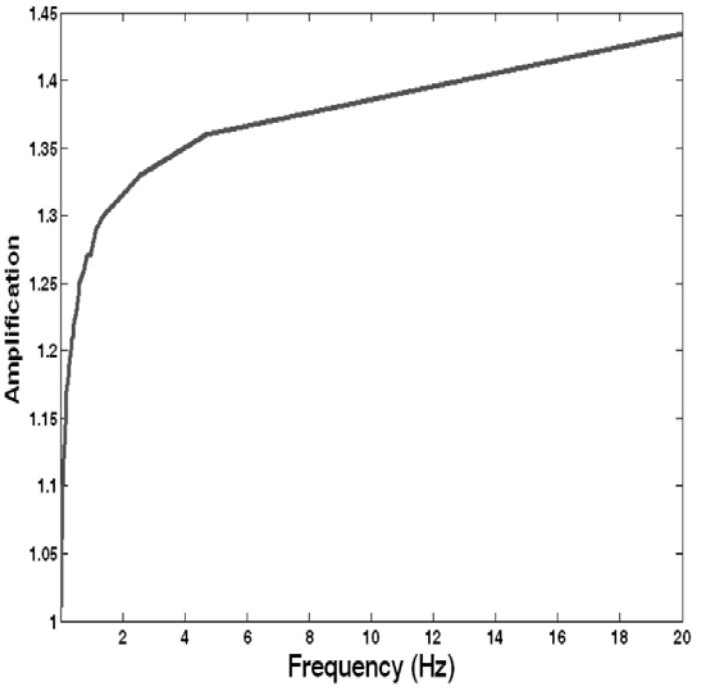

Figure 3. First-order approximated crustal amplification for the Darjeeling-Sikkim Himalaya.

Table 2. Generic source parameters for Darjeeling-Sikkim Himalaya corresponding to normal, reverse and strike-slip faulting earthquake mechanism, respectively considered for the generation of ground motion database amalgamating the synthetic with the observed events.

Parameters	Normal Fault	Strike-Slip Fault	Reverse Fault
Strike, Dip	187°, 59°	220°, 78°	310°, 35°
Stress drop	0.75-147 bar	0.75-147 bar	0.75-147 bar
Magnitude (M_w)	3.5-7.8	3.5-8.3	3.5-8.3
Hypocentral Depth (km)	15 km	47.4 km	26.4 km
Shear Wave Velocity	3.8 km/sec (Nath et al. 2005, Raj et al. 2009, Acton et al. 2011)		
Crustal Density	2.7 g/cm^3	2.7 g/cm^3	2.7 g/cm^3
Slip Distribution	Random	Random	Random
Quality factor	$167f^{0.47}$ (Nath et al. 2008)		
Kappa	0.02	0.02	0.02
Rupture length (km) Rupture width (km)	calculated using the formulations of Wells and Coppersmith (1994)		
Geometrical spreading	1/R (R<100 km) $1/R^{0.5}$ (R>100 km)		
Windowing function	Saragoni and Hart (1974)		
Damping	5		

wavelength approximation (Joyner and Boore 1981). The crustal amplification curve is shown in Figure 3.

Topography plays a vital role for sites located in the hilly terrain like Darjeeling-Sikkim Himalaya. In such areas, apart from incident wave we are expected to record diffracted and scattered waves that emanate from different parts of the hill which are hit upon by the incident waves (Nath et al. 2005, Nath et al. 2008). In regimes where constructive interference between incident and diffracted waves takes place, we observe site amplification and wherever destructive interference takes place amplitude gets reduced. Therefore, for the estimation of ground response at surface level from the recorded strong motion data it is essential to estimate site response/amplification. So, site

Table 3. Representative shallow crustal model for Darjeeling-Sikkim region (Acton et al. 2011) used for ground motion synthesis.

Depth (km)	Shear Wave Velocity (km/s)
0.5	2.94
1.0	2.91
1.5	3.10
2.0	3.15
2.5	3.31
3.5	3.55
4.0	3.50
5.7	3.50
6.1	3.37
8.0	3.37
9.9	3.37
10.0	3.34

response estimated by Thiruvengadam (2009) for different NEHRP site classes A, B, C and D as per elevation ranges is adopted here. The Site Amplification Factor, $HVSR_{ij}(f_k)$, is computed at each j^{th} site for the i^{th} event at the central frequency f_k from the root mean square average of the amplitude spectra of the transverse ($H_{ij}(f_k)|_T$) and the redial ($H_{ij}(f_k)|_R$) component respectively with respect to the Fourier spectra of the vertical component which read like $V_{ij}(f_k)$ (Nath et al. 2005).

$$HVSR_{ij}(f_k) = ((H_{ij}(f_k)|^2_T + H_{ij}(f_k)|^2_R)/2)^{0.5}/V_{ij}(f_k) \quad (8)$$

The representative generic site response curves of site classes A, B, C and D are depicted in Figure 4. In order to study the topographic effect on site amplification, the site response curves for site classes A and B are further subdivided according to station elevation. The site amplification for Darjeeling-Sikkim region varies from 2.5 to 8.5. We used this generic site response curves for systematic ground motion synthesis. Figure 5 depicts a satisfactory comparison between the recorded and the simulated acceleration spectrum of 2011 Sikkim Earthquake of M_w6.9 at Gangtok, Singtam, Mangan and Siliguri strong motion stations.

Next generation attenuation models:

The rapid estimation of ground motion parameters namely PGA, PGV and PSA at a site of interest are often achieved by using a ground motion prediction relationship that relates a specific ground motion parameter of ground shaking to one or more attributes of an earthquake (Campbell and Bozorgnia 2003, Nath et al. 2005, Nath et al. 2009, Abrahamson and Silva 1997). These parameters are found to increase with magnitude while decreasing with the epicenter distance and are also controlled by the fault-rupture directivity and site conditions. The Next Generation Prediction/Attenuation project was developed to propose a series of ground motion models intended for application to geographically diverse regions; the only constraint is that the region be tectonically active with earthquakes occurring in the shallow crust. However, these new equations have been purported to be valid for other regions of similar tectonics. The models are aimed at predicting different ground motion parameters namely PGA, PGV, and 5% damped PSA for 0.05−10 sec. Applicability of NGP has been tested and found reasonably suitable in several regions across the globe, e.g. Shoja–Taheri et al. (2010) in the Iranian Plateau, Stafford et al. (2008) in the Euro-Mediterranean region, and Campbell and Bozorgnia (2006) in Europe. In the present study, Boore and Atkinson (2008) and Campbell & Bozorgnia (2003) Ground Motion Prediction Models given in equations (9) and (14) respectively have been considered for the generation of NGP models for Darjeeling-Sikkim Himalaya for three tectonic faulting types viz. normal, reverse and strike-slip. The logic tree framework for surface consistent attenuation models pertaining to site classes-A, B, C and D at different elevation level is shown in Figure 6.

1) Boore and Atkinson 2008 (BA 08) ground motion prediction equation is given as,

$$\ln Y = F_M(M) + F_D(R_{JB}, M) + F_s(V_s^{30}, R_{JB}, M) + \sigma_t \quad (9)$$

The distance function is given by,

$$F_D(R_{JB}, M) = \left[c_1 + c_2(M - M_{ref})\right]\ln(R/R_{ref}) + c_3(R - R_{ref}) \quad (10)$$

$$R = \sqrt{R_{JB}^{\ 2} + h^2} \quad (11)$$

C_1, C_2, C_3, M_{ref}, R_{ref} and h are the co-efficient to be determined in the analysis and σ_t represent the standard deviation associated with prediction equation. The magnitude scaling is given by,

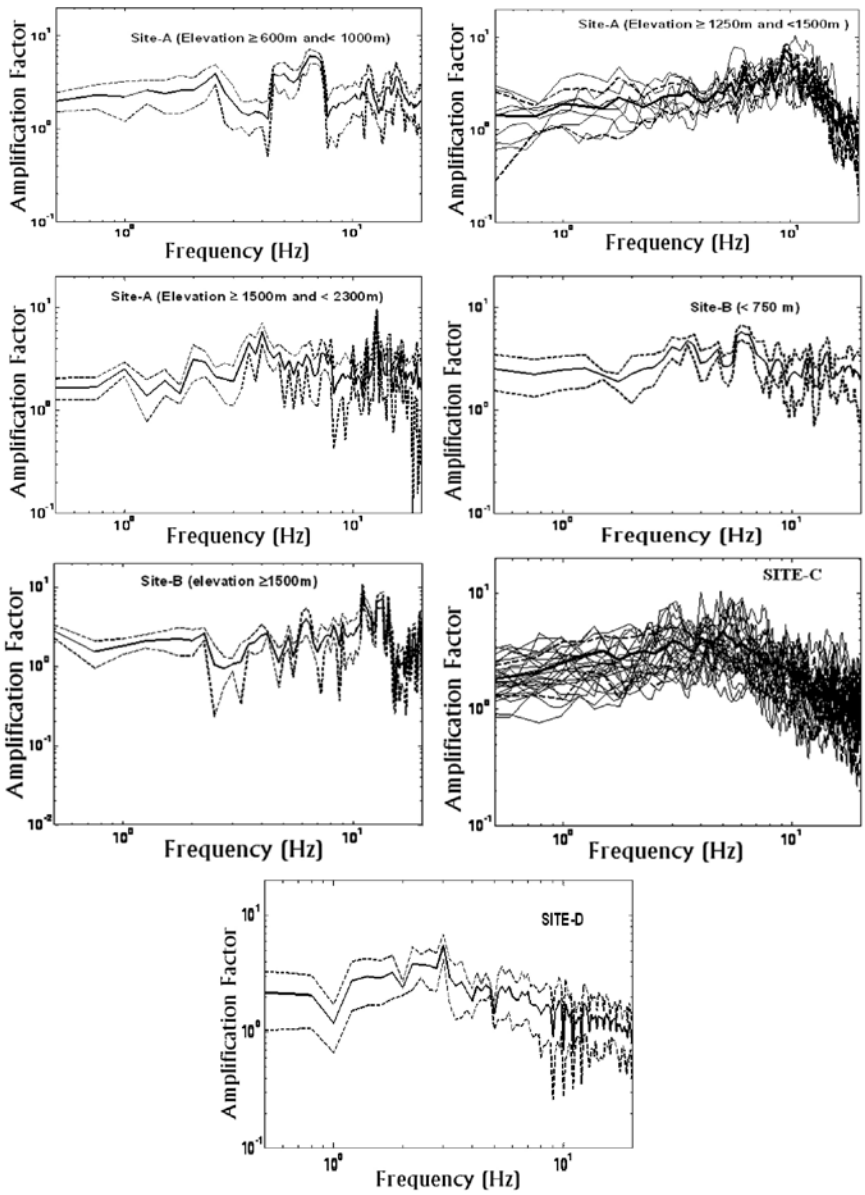

Figure 4. The average site amplification (bold line) for site classes A, B, C and D is represented. The ±1 standard deviation curve is shown as dotted lines. In order to study the topographic effect on site amplification, the site response curves for site class A and B are further sub-classified according to station elevation.

$$M \le M_h \quad F_M(M) = e_1 U + e_2 SS + e_3 NS + e_4 RS + e_5 (M - M_h) + e_6 (M - M_h)^2 \quad (12)$$

$$M > M_h \quad F_M(M) = e_1 U + e_2 SS + e_3 NS + e_4 RS + e_7 (M - M_h) \quad (13)$$

For bedrock surface $F_s(V_s^{30}, R_{jb}, M)$ is taken as zero. For strike-slip fault U=NS=RS=0 and SS=1; for normal fault U=NS=SS=0 and NS=1. Similarly for thrust fault U=NS=SS=0 and RS=1.

2) Campbell and Bozorgnia 2003 (CB 03) ground motion prediction equation is given as,

$$\ln Y = c_1 + f_1(M_w) + c_4 \ln\sqrt{f_2(M_w, r_{seis}, S)} + f_3(F) + f_4(S) + f_5(HW, F, M_w, r_{seis}) + e \quad (14)$$

where the magnitude scaling characteristics are given by,

$$f_1(M_w) = c_2 M_w + c_3 (8.5 - M_w)^2, \quad (15)$$

The distance scaling characteristics are given by,

$$f_2(M_w, r_{seis}, S) = r^2_{seis} + g(S)^2 (\exp[c_8 M_w + c_9 (8.5 - M_w)^2])^2, \quad (16)$$

in which the near-source effect of local site condition is given by,

$$g(S) = c_5 + c_6 (S_{VFS} + S_{SR}) + c_7 S_{FR}, \quad (17)$$

The effect of faulting mechanism is given by,

$$f_3(F) = c_{10} F_{RV} + c_{11} F_{TH}, \quad (18)$$

The far-source effect of local site conditions is given by,

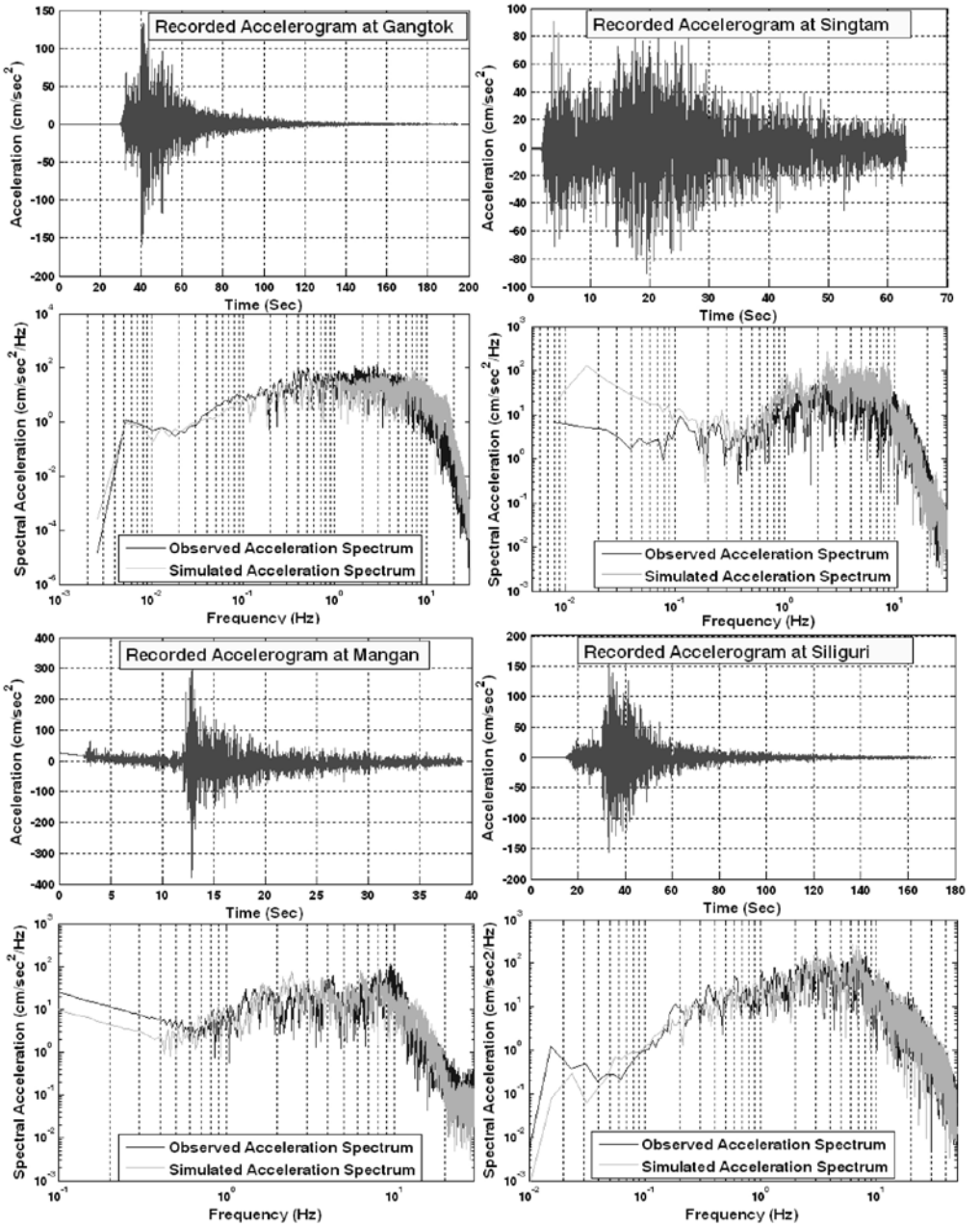

Figure 5. Recorded accelerogram, and comparison of the observed and simulated acceleration spectra of September, 2011 Sikkim Earthquake of M_w6.9 at Gangtok, Singtam, Mangan and Siliguri strong motion stations.

$$f_4(S) = c_{12}S_{VFS} + c_{13}S_{SR} + c_{14}S_{FR} \quad (19)$$

The effect of hanging wall is given by $f_5(HW,F,M_w,r_{seis})$. In the development of GMPE for Darjeeling-Sikkim region we neglect the effect of hanging wall. Y is PGA or 5% damped PSA in g or PGV in cm/sec. M_w is moment magnitude; r_{seis} is the closest distance to seismogenic rupture in km; r_{jb} is the closest distance to the surface projection of fault rupture in km. S_{VFS} = 1 for very firm soil, S_{SR}=1 for soft rock, S_{FR} =1 for firm rock, and S_{VFS} =S_{SR} =S_{FR} = 0 for firm soil; F_{RV} = 1 for reverse faulting, F_{TH} =1 for thrust faulting, and F_{RV} =F_{TH} =0 for strike-slip and normal faulting and e is a random error term with zero mean and standard deviation equal to σlnY.

The ground motion database for PGA and PSA has been generated by using stochastic simulation technique of a range of earthquakes of magnitude M_w 3.5 to the maximum credible magnitude of M_w 8.3 with an interval of M_w 0.2. Also the recorded events are amalgamated with the simulated ones with due validation to strengthen the strong motion data base. These equations are developed empirically by nonlinear regression of strong motion

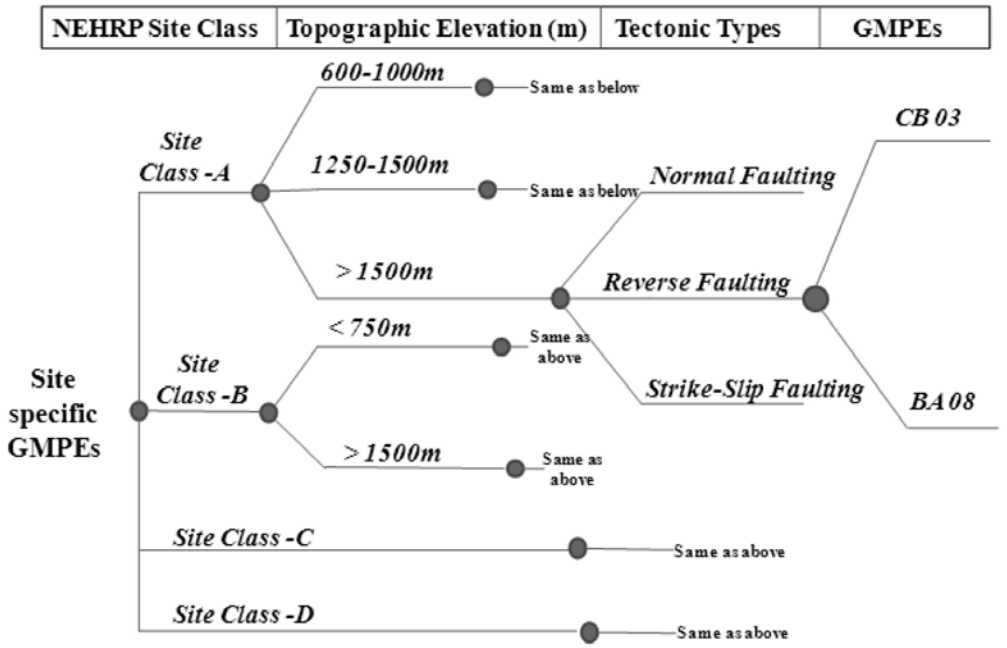

Figure 6. Logic tree framework for site specific surface consistent Next Generation Prediction Model of Darjeeling-Sikkim Himalaya.

amplitude data versus magnitude, distance, and other predictive variables. The non-linear regression analysis performed on the ground motion database of PGA, PSA for the three tectonic types have generated sets of regression coefficients as given in Tables 4 & 5 for both Boore and Atkinson (2008), Campbell and Bozorgnia (2003) models respectively.

RESULTS AND DISCUSSION

In the present Study NGP models have been developed based on the empirical formulation of Boore & Atkinson (2008) and Campbell & Bozorgnia (2003) Ground Motion Prediction Models for three tectonic types viz. normal faulting, strike-slip faulting and reverse faulting at the surface according to site classes A, B, C and D with different elevation ranges. Tables 4 and 5 present the coefficients for PGA and PSA at 0.2 and 1.0 sec of all the site classes. Figure 7 depicts the comparison between the observed/ simulated and the predicted peak ground acceleration as a function of fault rupture distance for different tectonic regimes based on Boore and Atkinson (2008) and Campbell and Bozorgnia (2003) NGP models. These comparisons provide satisfactory and unbiased prediction.

The regression models for the PGA and PSA have been validated using an analysis of residuals as,

$$\delta_i = \frac{\left(\ln Y_i - \overline{\ln Y_i}\right)}{\sigma_{\ln}} \qquad (20)$$

where, InY is the natural logarithm of i^{th} observed value of Y, $\overline{InY_i}$ is the natural logarithm of i^{th} predicted value of Y, and σ_{In} is the standard deviation of PGA or PSA of the ground motion. The intra-event residuals are normalized by σ_{In} in order to reduce the relative differences in the scatter in the intra-event residuals among the different strong motion parameters. The representative Residual plots for site class D for PGA and PSA at 0.2, 1.0 sec of ground motion as a function of rupture distance for normal, reverse and strike-slip tectonic type of earthquake mechanism are shown in Figure 8. It is evident from the diagram that the residuals have a zero mean with respect to the fault rupture distance. A residual analysis of PGA and PSA of the NGP models predicted in the present investigation are unbiased with respect to fault rupture distance and hence can be used along with other existing prediction equations in a logic tree frame work for the seismic hazard assessment of this earthquake prone territory of the Himalaya. A comparison of the PGA models derived for the empirical relations from Boore and Atkinson (2008) and Campbell & Bozorgnia (2003) of site classes C and D for three tectonic types shown in Figure 9 predict higher horizontal ground acceleration for reverse faulting as compared to the strike-slip and normal faulting earthquake mechanisms.

A preliminary study on the application of derived NGP models for the estimation of seismic hazard in Darjeeling-Sikkim Himalaya has been carried out. The seismic hazard assessment is concerned with getting an estimate of the strong-motion parameters at a site for the purpose of

Table 4. Regression Coefficients for Boore and Atkinson (2008) (BA 08) NGP model.

Site Class A: ≥600m and < 1000m Normal Fault															
PSA (Sec)	C_1	C_2	C_3	h	M_{ref}	R_{ref}	e_1	e_2	e_3	e_4	e_5	e_6	e_7	M_h	σ
0.2	-0.6215	0.1587	-0.0189	9.9226	4.5	1.2916	0.4613	0.4866	0.1277	0.4933	0.2134	-0.2056	0.0574	6.75	0.2356
1	-0.7944	0.2024	-0.0109	9.6973	4.5	0.45	0.4613	0.4866	0.0451	0.4933	0.0759	-0.594	-0.0883	6.75	0.2563
PGA	-0.7518	0.1811	-0.0148	13.1401	4.9	3.0328	-0.538	-0.5035	-0.5432	-0.5097	0.5391	-0.1178	0.1752	6.32	0.2356
Reverse Fault															
PSA (Sec)	C_1	C_2	C_3	h	M_{ref}	R_{ref}	e_1	e_2	e_3	e_4	e_5	e_6	e_7	M_h	σ
0.2	-0.5412	0.1481	-0.0174	8.9288	4.5	0.5717	0.5718	0.5925	0.4086	0.2954	0.1574	-0.2242	-0.1711	6.75	0.3560
1	-0.5481	0.1237	-0.0102	8.0256	4.5	0.5617	-0.469	-0.4344	-0.7846	-0.4337	0.9573	-0.1851	0.219	6.75	0.1254
PGA	-0.7401	0.2063	-0.0153	11.4337	4.6	2.2506	-0.538	-0.5035	-0.7547	-0.4587	0.0816	-0.2429	-0.112	6.74	0.3569
Strike-Slip Fault															
PSA (Sec)	C_1	C_2	C_3	h	M_{ref}	R_{ref}	e_1	e_2	e_3	e_4	e_5	e_6	e_7	M_h	σ
0.2	-0.7362	0.1135	-0.0135	13.0894	4.50	1.5622	0.4613	0.6525	0.3019	0.4933	0.3386	-0.2191	0.0509	6.75	0.3560
1	-1.1465	0.1247	-0.0033	19.9599	4.50	1.4444	0.4613	1.0521	0.3019	0.4933	0.9533	-0.2083	0.1563	6.75	0.4589
PGA	-0.8564	0.1586	-0.0094	16.9052	5.98	3.9669	-0.538	0.0207	-0.7547	-0.5097	-0.1618	-0.198	3.8376	7.79	0.3560
Site Class A: ≥1250m and < 1500m Normal Fault															
PSA (Sec)	C_1	C_2	C_3	h	M_{ref}	R_{ref}	e_1	e_2	e_3	e_4	e_5	e_6	e_7	M_h	σ
0.2	-0.7048	0.1237	-0.018	13.0759	4.5	3.93	0.4613	0.4866	0.6584	0.4933	0.4021	-0.1984	0.2251	6.75	0.254
1	-0.8707	0.1336	-0.0068	12.9085	4.5	0.6429	0.4613	0.4866	0.4025	0.4933	0.7474	-0.1968	0.0888	6.75	0.152
PGA	-0.7577	0.1554	-0.0141	13.6694	5.2	5.2487	-0.538	-0.5035	-0.4234	-0.5097	0.1891	-0.2198	0.189	6.89	0.256
Reverse Fault															
PSA (Sec)	C_1	C_2	C_3	h	M_{ref}	R_{ref}	e_1	e_2	e_3	e_4	e_5	e_6	e_7	M_h	σ
0.2	-0.4975	0.1437	-0.0194	7.3309	4.5	1.0913	0.5718	0.5925	0.4086	0.5706	0.4258	-0.1462	-0.0588	6.75	0.2356
1	-1.4789	0.2389	-0.0043	12.5459	4.5	4.4602	-0.469	-0.4344	-0.7846	0.1456	0.8556	-0.2338	0.0797	6.75	0.2456
PGA	-0.7522	0.1935	-0.0155	11.4982	4.5	1.7625	-0.538	-0.5035	-0.7547	-0.4037	-0.3106	-0.2514	-0.0856	7.43	0.2563
Strike-Slip Fault															
PSA (Sec)	C_1	C_2	C_3	h	M_{ref}	R_{ref}	e_1	e_2	e_3	e_4	e_5	e_6	e_7	M_h	σ
0.2	-0.73	0.1212	-0.0134	13.2397	4.5	1.5791	0.4613	0.6683	0.3019	0.4933	0.1911	-0.2874	0.0669	6.75	0.352
1	-1.264	0.13	-0.0029	12.3127	4.5	1.53	0.4613	1.1788	0.3019	0.4933	0.7965	-0.2953	0.182	6.75	0.220
PGA	-0.9781	0.1856	-0.007	19.9529	6.64	5.0542	-0.538	0.2597	-0.7547	-0.5097	-0.1467	-0.1786	4.1994	7.79	0.1520
Site Class A: ≥1500m and < 2300m Normal Fault															
PSA (Sec)	C_1	C_2	C_3	h	M_{ref}	R_{ref}	e_1	e_2	e_3	e_4	e_5	e_6	e_7	M_h	σ
0.2	-0.7774	0.1284	-0.0151	13.1821	4.5	0.7545	0.4613	0.4866	0.9858	0.4933	0.1947	-0.2166	0.0207	6.75	0.1256
1	-0.957	0.148	-0.0069	13.6253	4.5	0.8876	0.4613	0.4866	0.5163	0.4933	0.6978	-0.1986	0.0714	6.75	0.1230
PGA	-0.7896	0.1507	-0.0115	15.0657	5.5	4.8316	-0.538	-0.5035	-0.3737	-0.5097	0.1725	-0.2372	0.2091	6.99	0.2453
Reverse Fault															
PSA (Sec)	C_1	C_2	C_3	h	M_{ref}	R_{ref}	e_1	e_2	e_3	e_4	e_5	e_6	e_7	M_h	σ
0.2	-1.9411	0.4719	-0.0113	20.1626	4.5	8.4086	0.5188	0.535	0.3388	0.9148	1.4454	0.4395	-0.7143	6.75	0.2453
1	-1.2275	0.226	-0.0063	19.2519	4.5	3.4526	-0.469	-0.4344	-0.7846	0.0299	0.7936	-0.1929	0.0722	6.75	0.2563
PGA	-0.9185	0.281	-0.0122	16.2628	5.4	5.9338	-0.538	-0.5035	-0.7547	-0.3911	0.4529	-0.1435	-0.1217	6.5273	0.3523
Strike-Slip Fault															
PSA (Sec)	C_1	C_2	C_3	h	M_{ref}	R_{ref}	e_1	e_2	e_3	e_4	e_5	e_6	e_7	M_h	σ
0.2	-0.7127	0.1087	-0.0136	12.1835	4.5	1.3217	0.4613	0.6096	0.3019	0.4933	0.2016	-0.2965	0.084	6.75	0.3564
1	-1.3947	0.1557	-0.0022	21.8758	4.5	1.8303	0.4613	1.3082	0.3019	0.4933	0.5381	-0.3745	0.0939	6.75	0.2563
PGA	-0.9157	0.1832	-0.0086	17.2081	6.1	4.0101	-0.538	0.0498	-0.7547	-0.5097	0.0679	-0.2927	0.0658	6.68	0.3256
Site Class B: <700m Normal Fault															
PSA (Sec)	C_1	C_2	C_3	h	M_{ref}	R_{ref}	e_1	e_2	e_3	e_4	e_5	e_6	e_7	M_h	σ
0.2	-0.7505	0.1397	-0.015	11.5987	4.5	2.0705	0.4613	0.4866	0.4851	0.4933	0.3069	-0.2261	0.096	6.75	0.3890
1	-1.0294	0.1674	-0.0063	15.0861	4.5	1.619	0.4613	0.4866	0.5633	0.4933	0.5005	-0.4302	0.1105	6.75	0.2320
PGA	-0.8763	0.2028	-0.0111	16.0707	5.6	5.4826	-0.538	-0.5035	-0.31	-0.5097	0.0552	-0.2639	0.151	7.00	0.3685

Reverse Fault															
PSA (Sec)	C_1	C_2	C_3	h	M_{ref}	R_{ref}	e_1	e_2	e_3	e_4	e_5	e_6	e_7	M_h	σ
0.2	-0.7455	0.1959	-0.0169	12.0785	4.5	1.6977	0.5718	0.5925	0.4086	0.4766	0.1212	-0.2534	-0.1635	6.75	0.3896
1	-1.5435	0.2109	-0.0033	13.6202	4.5	5.9624	-0.469	-0.4344	-0.7846	0.3723	1.0649	-0.1288	0.1859	6.75	0.3698
PGA	-0.8188	0.1943	-0.0139	1.5787	4.7	1.4839	-0.538	-0.5035	-0.7547	0.0188	0.5448	-0.081	-0.1232	6.22	0.3850
Strike-Slip Fault															
PSA (Sec)	C_1	C_2	C_3	h	M_{ref}	R_{ref}	e_1	e_2	e_3	e_4	e_5	e_6	e_7	M_h	σ
0.2	-0.6927	0.096	-0.0134	12.4911	4.5	1.7358	0.4613	0.6739	0.3019	0.4933	0.3165	-0.2599	0.1627	6.75	0.3856
1	-1.4395	0.1468	-0.0019	12.5757	4.5	2.5453	0.4613	1.2669	0.3019	0.4933	0.6283	-0.3824	0.1875	6.75	0.3963
PGA	-0.9593	0.1948	-0.0072	18.6456	6.4156	5.0316	-0.538	0.1544	-0.7547	-0.5097	0.0951	-0.3467	0.095	6.5651	0.3752
Site Class B: > 1500m Normal Fault															
PSA (Sec)	C_1	C_2	C_3	h	M_{ref}	R_{ref}	e_1	e_2	e_3	e_4	e_5	e_6	e_7	M_h	σ
0.2	-0.6742	0.1696	-0.0182	9.2701	4.5	2.2957	0.4613	0.4866	0.5073	0.4933	0.1651	-0.2541	0.0651	6.75	0.3235
1	-0.8043	0.1853	-0.011	10.2931	4.5	0.3391	0.4613	0.4866	0.0527	0.4933	0.3059	-0.3572	-0.098	6.75	0.3457
PGA	-0.7172	0.1626	-0.0162	12.1099	4.8	4.0519	-0.538	-0.5035	-0.619	-0.5097	0.3383	-0.1929	0.2076	6.55	0.3365
Reverse Fault															
PSA (Sec)	C_1	C_2	C_3	h	M_{ref}	R_{ref}	e_1	e_2	e_3	e_4	e_5	e_6	e_7	M_h	σ
0.2	-0.3819	0.1057	-0.0195	7.2085	4.5	0.4912	0.5718	0.5925	0.4086	0.5061	-0.1028	-0.4156	0.0656	6.75	0.3854
1	-1.0553	0.2229	-0.0084	14.1335	4.5	2.6564	-0.469	-0.4344	-0.7846	-0.3598	1.2326	0.0702	-0.004	6.75	0.3421
PGA	-0.7118	0.1865	-0.0158	11.1331	4.5	1.6278	-0.538	-0.5035	-0.7547	-0.4339	-0.2734	-0.253	-0.0822	7.30	0.3356
Strike-Slip Fault															
PSA (Sec)	C_1	C_2	C_3	h	M_{ref}	R_{ref}	e_1	e_2	e_3	e_4	e_5	e_6	e_7	M_h	σ
0.2	-0.7517	0.1122	-0.0154	13.3512	4.5	3.8261	0.4613	0.7854	0.3019	0.4933	0.3698	-0.267	0.1835	6.75	0. 1245
1	-1.2005	0.1315	-0.0026	20.4203	4.5	1.0272	0.4613	1.1413	0.3019	0.4933	0.6407	-0.2987	0.1056	6.75	0.38563
PGA	-0.889	0.1556	-0.009	17.5618	6.2	4.3842	-0.538	0.1423	-0.7547	-0.5097	-0.1159	-0.187	0.2201	7.74	0. 1452
Site Class C: Normal Fault															
PSA (Sec)	C_1	C_2	C_3	h	M_{ref}	R_{ref}	e_1	e_2	e_3	e_4	e_5	e_6	e_7	M_h	σ
0.2	-2.0814	0.2333	-0.0059	29.5707	4.5	10.534	0.4613	0.4866	1.4915	0.4933	0.4109	-0.1651	0.2408	6.75	0. 161
1	-2.3662	0.2904	0.0023	32.1828	4.5	5.3893	0.4613	0.4866	1.7032	0.4933	0.4976	-0.3142	0.1151	6.75	0.1419
PGA	-1.3111	0.3053	-0.0043	27.6054	7.303	11.549	-0.538	-0.5035	0.2687	-0.5097	0.1488	-0.1609	0.1489	7.18	0.1533
Reverse Fault															
PSA (Sec)	C_1	C_2	C_3	h	M_{ref}	R_{ref}	e_1	e_2	e_3	e_4	e_5	e_6	e_7	M_h	σ
0.2	-1.3466	0.2023	-0.0103	22.2811	4.5	5.9917	0.5718	0.5925	0.4086	1.2351	0.3316	-0.2217	0.0794	6.75	0.1323
1	-2.9083	0.3228	0.0065	39.3172	4.5	11.581	-0.469	-0.4344	-0.7846	1.1688	0.8223	-0.2317	0.1617	6.75	0.1243
PGA	-1.1234	0.2524	-0.0065	24.5612	6.660	7.2606	-0.538	-0.5035	-0.7547	0.3046	-0.1237	-0.2295	0.0725	7.33	0.1431
Strike-Slip Fault															
PSA (Sec)	C_1	C_2	C_3	h	M_{ref}	R_{ref}	e_1	e_2	e_3	e_4	e_5	e_6	e_7	M_h	σ
0.2	-0.8972	0.123	-0.0128	15.9137	4.5	4.0245	0.4613	0.8602	0.3019	0.4933	0.2602	-0.2936	0.1569	6.75	0.1303
1	-1.1429	0.1198	-0.0033	19.2466	4.5	1.2912	0.4613	1.1022	0.3019	0.4933	0.752	-0.2874	0.2016	6.75	0.1203
PGA	-0.7294	0.1385	-0.0131	13.359	5.120	2.7355	-0.538	-0.1845	-0.7547	-0.5097	0.0356	-0.2302	0.0738	7.00	0.1331
Site Class D: Normal Fault															
PSA (Sec)	C_1	C_2	C_3	h	M_{ref}	R_{ref}	e_1	e_2	e_3	e_4	e_5	e_6	e_7	M_h	σ
0.2	-1.8337	0.2325	-0.0071	26.679	4.5	7.3874	0.4613	0.4866	1.124	0.4933	0.3262	-0.1811	0.1672	6.75	0.1256
1	-2.3777	0.3055	0.0016	31.3972	4.5	4.4112	0.4613	0.4866	1.7766	0.4933	0.3864	-0.3157	0.005	6.75	0.369
PGA	-1.205	0.2857	-0.005	25.7212	7.0	8.3222	-0.538	-0.5035	0.2003	-0.5097	0.1278	-0.1853	0.1279	7.0	0.125
Reverse Fault															
PSA (Sec)	C_1	C_2	C_3	h	M_{ref}	R_{ref}	e_1	e_2	e_3	e_4	e_5	e_6	e_7	M_h	σ
0.2	-1.3451	0.1988	-0.0103	22.2652	4.5	5.9762	0.5718	0.5925	0.4086	1.2342	0.2964	-0.2621	0.0806	6.75	0.145
1	-2.8921	0.3132	0.0065	39.317	4.5	11.584	-0.469	-0.4344	-0.7846	1.169	0.8186	-0.2359	0.1613	6.75	0.157
PGA	-1.1158	0.2819	-0.0065	24.5846	6.6	6.7986	-0.538	-0.5035	-0.7547	0.3715	-0.1449	-0.2374	0.0565	7.31	0.3458
Strike-Slip Fault															
PSA (Sec)	C_1	C_2	C_3	h	M_{ref}	R_{ref}	e_1	e_2	e_3	e_4	e_5	e_6	e_7	M_h	σ
0.2	-1.0572	0.1329	-0.0103	17.7735	4.5	2.6031	0.4613	0.9762	0.3019	0.4933	0.163	-0.3034	0.0727	6.75	0.3458
1	-1.0875	0.1188	-0.0043	17.536	4.5	0.8602	0.4613	1.0197	0.3019	0.4933	0.635	-0.3004	0.1269	6.75	0.3789
PGA	-0.8184	0.1528	-0.0099	15.79	5.7	2.8381	-0.538	-0.0895	-0.7547	-0.5097	0.0069	-0.2341	0.035	7.00	0.3896

Table 5. Regression coefficients for Campbell and Bozorgnia (2003) (CB 03) NGP model.

Site Class A: ≥600m and < 1000m Normal Fault															
PSA (Sec)	C_1	C_2	C_3	C_4	C_5	C_6	C_7	C_8	C_9	C_{10}	C_{11}	C_{12}	C_{13}	C_{14}	σ
0.2	0.9862	0.4477	-0.142	-2.142	14.798	-0.014	14.6622	0.022	-0.0761	0.296	0.34	-0.14	-0.18	3.3981	0.330
1	-1.652	0.6227	-0.187	-1.465	-8.518	0	-8.537	-0.334	-0.3737	0.329	0.33	-0.07	-0.07	1.5468	0.321
PGA	-0.520	0.5296	-0.135	-2.025	12.855	-0.005	12.7969	0.0429	-0.0834	0.343	0.35	-0.12	-0.13	3.2238	0.335
Reverse Fault															
PSA (Sec)	C_1	C_2	C_3	C_4	C_5	C_6	C_7	C_8	C_9	C_{10}	C_{11}	C_{12}	C_{13}	C_{14}	σ
0.2	0.0859	0.203	-0.184	-1.998	4.5971	-0.014	4.461	0.1764	-0.0234	3.172	0.34	-0.14	-0.18	2.5179	0.3324
1.0	-2.983	0.1813	-0.232	-0.889	-1.9533	0.41	-1.9723	-5.005	-95.876	2.452	0.33	-0.07	-0.07	1.2654	0.2535
PGA	-1.303	0.2222	-0.195	-1.808	6.7166	-0.005	6.6627	0.1235	-0.0726	3.082	0.35	-0.12	-0.13	2.4505	0.3525
Strike-Slip Fault															
PSA (Sec)	C_1	C_2	C_3	C_4	C_5	C_6	C_7	C_8	C_9	C_{10}	C_{11}	C_{12}	C_{13}	C_{14}	σ
0.2	2.1577	-0.168	-0.249	-1.699	11.786	-0.014	11.5584	-0.142	-0.1175	0.296	0.34	-0.14	-0.18	4.7696	0.25145
1	1.069	-0.240	-0.357	-1.214	4.5112	0	4.4921	-0.154	-0.1831	0.329	0.33	-0.07	-0.07	4.2479	0.21250
PGA	-0.477	0.0127	-0.216	-1.650	16.452	-0.005	16.3921	-0.016	-0.1012	0.343	0.35	-0.12	-0.13	4.3412	0.22145
Site Class A: ≥1250m and < 1500m Normal Fault															
PSA (Sec)	C_1	C_2	C_3	C_4	C_5	C_6	C_7	C_8	C_9	C_{10}	C_{11}	C_{12}	C_{13}	C_{14}	σ
0.2	1.8051	0.3276	-0.149	-2.365	4.4874	-0.014	4.3514	0.0224	-0.0479	0.296	0.34	-0.14	-0.18	4.5571	0.23145
1	0.1238	0.0155	-0.289	-1.261	9.1358	0	9.1168	-0.566	-0.3675	0.329	0.33	-0.07	-0.07	3.2528	0.2547
PGA	0.4832	0.2972	-0.157	-2.099	12.662	-0.005	12.6034	0.0302	-0.0604	0.343	0.35	-0.12	-0.13	4.2271	0.2540
Reverse Fault															
PSA (Sec)	C_1	C_2	C_3	C_4	C_5	C_6	C_7	C_8	C_9	C_{10}	C_{11}	C_{12}	C_{13}	C_{14}	σ
0.2	-0.05	0.446	-0.126	-2.236	0.7934	-0.014	0.6574	0.4229	0.0598	3.077	0.34	-0.14	-0.18	2.422	0.2625
1.0	-2.242	-0.105	-0.292	-0.916	-1.1305	0	-1.1495	-3.474	-0.5313	3.153	0.33	-0.07	-0.07	1.9666	0.3335
PGA	-1.275	0.2111	-0.190	-1.821	5.3085	-0.005	5.2494	0.1474	-0.0561	3.125	0.35	-0.12	-0.13	2.4936	0.3145
Strike-Slip Fault															
PSA (Sec)	C_1	C_2	C_3	C_4	C_5	C_6	C_7	C_8	C_9	C_{10}	C_{11}	C_{12}	C_{13}	C_{14}	σ
0.2	1.5889	-0.032	-0.214	-1.678	2.6962	-0.014	2.4637	-0.096	-0.1137	0.296	0.34	-0.14	-0.18	4.1909	0.3332
1	0.2427	-0.017	-0.289	-1.225	-1.0391	0	-1.0581	0.3147	-0.0052	0.329	0.33	-0.07	-0.07	3.3917	0.3042
PGA	0.2994	0.1142	-0.191	-1.697	8.5006	-0.005	8.4415	0.0707	-0.0778	0.343	0.35	-0.12	-0.13	4.0433	0.3245
Site Class A: ≥1500m and < 2300m Normal Fault															
PSA (Sec)	C_1	C_2	C_3	C_4	C_5	C_6	C_7	C_8	C_9	C_{10}	C_{11}	C_{12}	C_{13}	C_{14}	σ
0.2	0.6735	0.6242	-0.067	-2.306	1.2653	-0.014	1.1293	0.349	0.0629	0.296	0.34	-0.14	-0.18	3.1155	0.3135
1	-1.652	0.6227	-0.187	-1.465	-2.518	0	-2.537	-0.334	-0.3737	0.329	0.33	-0.07	-0.07	1.5468	0.3036
PGA	-0.145	0.3934	-0.138	-2.000	3.2513	-0.005	3.1923	0.2046	-0.0035	0.343	0.35	-0.12	-0.13	3.6147	0.2934
Reverse Fault															
PSA (Sec)	C_1	C_2	C_3	C_4	C_5	C_6	C_7	C_8	C_9	C_{10}	C_{11}	C_{12}	C_{13}	C_{14}	σ
0.2	-0.623	0.5299	-0.033	-2.038	2.0645	-1.014	2.9284	-0.247	-11.481	1.953	0.34	-0.14	-0.18	1.2989	0.2825
1.0	-2.172	-0.112	-0.293	-0.934	-0.2876	0	-0.3066	-0.945	-0.6739	3.203	0.33	-0.07	-0.07	2.0166	0.2445
PGA	-1.9068	-0.1585	-0.2189	-1.1178	0.9035	0	0.8845	-2.6392	-1.2046	3.2759	0.021	-0.154	-0.117	2.4672	0.2152
Strike-Slip Fault															
PSA (Sec)	C_1	C_2	C_3	C_4	C_5	C_6	C_7	C_8	C_9	C_{10}	C_{11}	C_{12}	C_{13}	C_{14}	σ
0.2	1.5439	-0.0628	-0.2186	-1.6014	1.9463	-0.014	1.8092	-0.1974	-0.1544	0.296	0.342	-0.148	-0.183	4.1159	0.25645
1	0.5759	-0.088	-0.3024	-1.3069	4.2316	0	4.2126	-0.1625	-0.1924	0.329	0.338	-0.073	-0.072	3.7748	0.24175
PGA	0.7477	0.0622	-0.2005	-1.6044	13.3693	-0.009	13.8879	-0.1209	-0.1537	0.224	0.313	-0.146	-0.253	3.3506	0.2684
Site Class B: <700m Normal Fault															
PSA (Sec)	C_1	C_2	C_3	C_4	C_5	C_6	C_7	C_8	C_9	C_{10}	C_{11}	C_{12}	C_{13}	C_{14}	σ
0.2	0.9822	0.4605	-0.1198	-2.1557	2.3284	-0.014	2.1925	0.2603	0.0042	0.296	0.342	-0.148	-0.183	3.4142	0.2342
1	-0.8974	0.0274	-0.2438	-1.0069	-6.0529	0	-6.0719	-5.5777	-2.8794	0.329	0.338	-0.073	-0.072	3.3216	0.2525
PGA	0.0177	0.3283	-0.1715	-1.9174	15.4535	-0.005	15.3946	0.0104	-0.0994	0.343	0.351	-0.123	-0.138	3.7616	0.2424

Reverse Fault															
PSA (Sec)	C_1	C_2	C_3	C_4	C_5	C_6	C_7	C_8	C_9	C_{10}	C_{11}	C_{12}	C_{13}	C_{14}	σ
0.2	0.0754	0.2998	-0.1654	-2.131	2.9959	-0.014	2.8599	0.2454	-0.0065	3.1724	0.342	-0.148	-0.183	2.5174	0.3630
1.0	-1.8386	0.0518	-0.2958	-1.3861	-3.561	0	-3.58	-0.0537	-0.144	3.5623	0.338	-0.073	-0.072	2.3753	0.3234
PGA	-3.2167	-0.0167	-0.1885	-1.1139	0.2032	-0.005	0.1442	-0.3024	-17.2872	3.3392	0.351	-0.123	-0.138	2.7072	0.2245
Strike-Slip Fault															
PSA (Sec)	C_1	C_2	C_3	C_4	C_5	C_6	C_7	C_8	C_9	C_{10}	C_{11}	C_{12}	C_{13}	C_{14}	σ
0.2	1.549	-0.0115	-0.2058	-1.6634	4.5019	-0.014	4.303	-0.0392	-0.0821	0.296	0.342	-0.148	-0.183	4.151	0.3025
1	1.329	-0.2406	-0.3575	-1.2148	4.5112	0	4.4921	-0.1542	-0.1831	0.329	0.338	-0.073	-0.072	4.2479	0.3220
PGA	0.5698	-0.028	-0.2245	-1.6113	4.8518	-0.005	4.7871	-0.248	-0.1796	0.343	0.351	-0.123	-0.138	4.4538	0.3516
Site Class B: >1500m Normal Fault															
PSA (Sec)	C_1	C_2	C_3	C_4	C_5	C_6	C_7	C_8	C_9	C_{10}	C_{11}	C_{12}	C_{13}	C_{14}	σ
0.2	-1.0044	0.8601	-0.0397	-1.9264	11.8651	-0.014	11.7291	-0.2322	-0.3042	0.296	0.342	-0.148	-0.183	1.5776	0.3025
1	-2.2115	0.7825	-0.0964	-1.558	0.0146	0	-0.0044	1.0245	0.2369	0.329	0.338	-0.073	-0.072	0.9175	0.3945
PGA	-0.2358	0.4307	-0.132	-2.0125	13.3967	-0.005	13.3377	0.0201	-0.0776	0.343	0.351	-0.123	-0.138	3.5181	0.3525
Reverse Fault															
PSA (Sec)	C_1	C_2	C_3	C_4	C_5	C_6	C_7	C_8	C_9	C_{10}	C_{11}	C_{12}	C_{13}	C_{14}	σ
0.2	0.2598	0.2125	-0.1778	-2.2728	10.3807	-0.014	10.8449	-0.0323	-0.0609	3.7167	0.342	-0.148	-0.183	3.0617	0.3435
1.0	-2.0728	-0.1572	-0.3032	-0.9916	-4.152	0	-4.1712	-11.347	-213.313	3.3233	0.338	-0.073	-0.072	2.1363	0.3125
PGA	-1.1551	0.1783	-0.1964	-1.8512	11.598	-0.005	11.5389	0.0477	-0.0784	3.2409	0.351	-0.123	-0.138	2.6089	0.3436
Strike-Slip Fault															
PSA (Sec)	C_1	C_2	C_3	C_4	C_5	C_6	C_7	C_8	C_9	C_{10}	C_{11}	C_{12}	C_{13}	C_{14}	σ
0.2	1.8687	0.0795	-0.1896	-1.8268	6.2059	-0.014	6.0698	0.1051	-0.0484	0.296	0.342	-0.148	-0.183	4.3207	0. 256
1	-1.0066	-0.2059	-0.2992	-0.8837	0.1637	0	0.1447	-5.4882	-0.1011	0.329	0.338	-0.073	-0.072	4.2023	0. 369
PGA	0.5739	0.0275	-0.2082	-1.6859	13.9666	-0.005	13.9026	0.0015	-0.0949	0.343	0.351	-0.123	-0.138	4.3477	0.3647
Site Class C: Normal Fault															
PSA (Sec)	C_1	C_2	C_3	C_4	C_5	C_6	C_7	C_8	C_9	C_{10}	C_{11}	C_{12}	C_{13}	C_{14}	σ
0.2	0.6249	0.7223	-0.0474	-2.3885	1.3467	-0.014	1.2108	0.3376	0.0509	0.296	0.342	-0.148	-0.183	3.0369	0.1654
1	-1.6763	0.223	-0.1998	-1.0033	0.7403	0.3235	0.7213	-0.9943	-29.5661	0.329	0.338	-0.073	-0.072	2.3727	0.3458
PGA	-0.7777	0.5937	-0.1002	-2.0382	2.2429	-0.005	2.1839	0.2578	-0.0099	0.343	0.351	-0.123	-0.138	2.9662	0.3363
Reverse Fault															
PSA (Sec)	C_1	C_2	C_3	C_4	C_5	C_6	C_7	C_8	C_9	C_{10}	C_{11}	C_{12}	C_{13}	C_{14}	σ
0.2	0.5177	0.0617	-0.218	-1.958	31.0215	-0.014	30.8855	-0.08	-0.1066	3.584	0.34	-0.14	-0.18	2.9296	0.2159
1.0	-2.336	-0.048	-0.275	-0.922	-0.0749	0	-0.0939	-1.129	-36.846	3.039	0.33	-0.07	-0.07	1.8527	0.4559
PGA	-3.280	0.012	-0.174	-1.131	0.1906	-0.405	0.4316	-0.922	-24.032	3.255	0.35	-0.12	-0.13	2.6234	0.1579
Strike-Slip Fault															
PSA (Sec)	C_1	C_2	C_3	C_4	C_5	C_6	C_7	C_8	C_9	C_{10}	C_{11}	C_{12}	C_{13}	C_{14}	σ
0.2	2.1826	-0.007	-0.208	-1.825	19.0477	-0.014	18.9115	-0.0328	-0.0866	0.296	0.342	-0.148	-0.183	4.6045	0.2159
1	0.4718	-0.047	-0.300	-1.257	774.451	0	774.4328	-0.5222	-0.3384	0.329	0.338	-0.073	-0.072	3.5308	0.4559
PGA	0.38	0.0508	-0.201	-1.639	58.9839	-0.005	58.9199	-0.1824	-0.175	0.343	0.351	-0.123	-0.138	4.152	0.3528
Site Class D: Normal Fault															
PSA (Sec)	C_1	C_2	C_3	C_4	C_5	C_6	C_7	C_8	C_9	C_{10}	C_{11}	C_{12}	C_{13}	C_{14}	σ
0.2	0.9476	0.4255	-0.1388	-2.1117	17.6536	-0.014	17.5177	-0.0075	-0.0795	0.296	0.342	-0.148	-0.183	3.3595	0.1654
1	-4.0716	1.8143	-0.0231	-1.9818	55.5093	-0.033	55.2207	-0.0489	-0.319	0.318	0.344	-0.176	-0.267	-2.1356	0.3458
PGA	-0.8929	0.4843	-0.1337	-1.8191	15.2906	-0.005	15.2316	0.0025	-0.111	0.343	0.351	-0.123	-0.138	2.8511	0.3363
Reverse Fault															
PSA (Sec)	C_1	C_2	C_3	C_4	C_5	C_6	C_7	C_8	C_9	C_{10}	C_{11}	C_{12}	C_{13}	C_{14}	σ
0.2	0.6	0.0212	-0.2317	-1.9461	50.2143	-0.014	50.0782	-0.1419	-0.1298	3.673	0.342	-0.148	-0.183	3.018	0.2159
1.0	-2.0907	-0.0892	-0.276	-0.9226	-0.0748	0	-0.0938	-1.1176	-36.6048	3.0413	0.338	-0.073	-0.072	1.8543	0.4559
PGA	-3.205	0.0545	-0.1776	-1.231	0.1906	-0.005	0.1316	-0.7227	-24.0331	3.2784	0.351	-0.123	-0.138	2.6464	0.1579
Strike-Slip Fault															
PSA (Sec)	C_1	C_2	C_3	C_4	C_5	C_6	C_7	C_8	C_9	C_{10}	C_{11}	C_{12}	C_{13}	C_{14}	σ
0.2	1.9692	-0.0556	-0.2254	-1.7618	58.5346	-0.014	58.3985	-0.1789	-0.1362	0.096	0.342	-0.148	-0.183	4.4612	0.2159
1	-2.7969	1.4058	-0.1377	-2.0481	1.9087	0.2356	1.5901	0.3994	-0.0936	0.329	0.338	-0.073	-0.072	0.2121	0.4559
PGA	0.0245	0.0893	-0.1995	-1.5623	74.5821	-0.005	74.5198	-0.2111	-0.1991	0.343	0.351	-0.123	-0.138	3.7638	0.3528

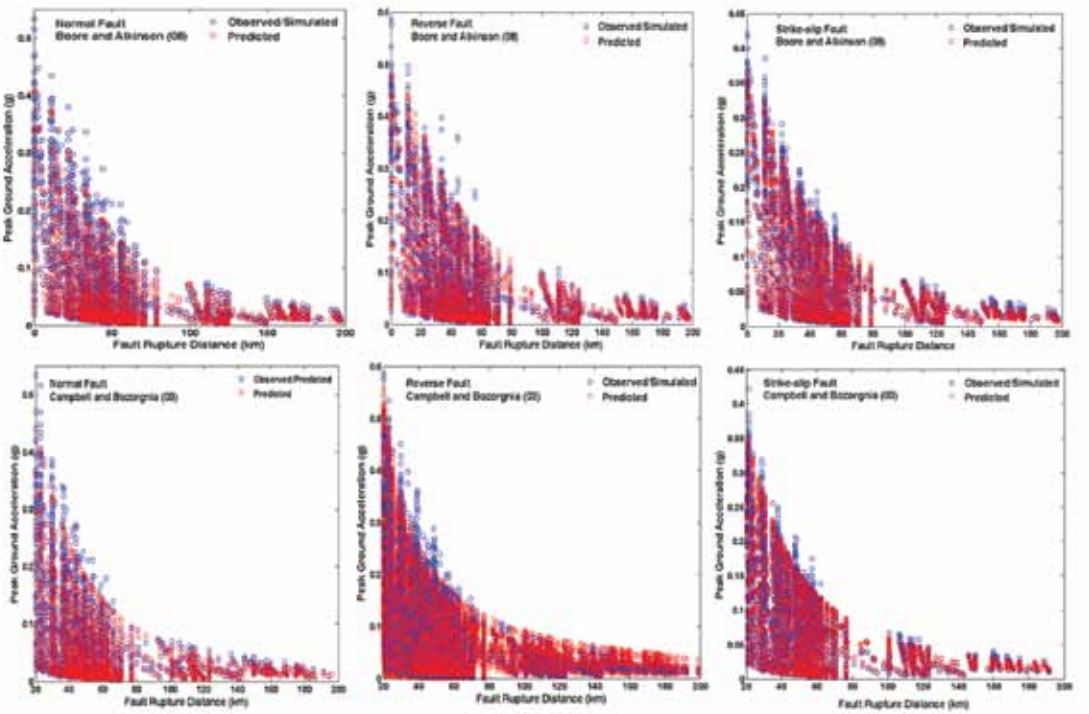

Figure 7. Observed and Simulated vs Predicted Peak Ground Acceleration for different tectonic types viz. normal fault, reverse fault, strike-slip faulting based on Boore and Atkinson (2008) and Campbell and Bozorgnia (2003) NGP models.

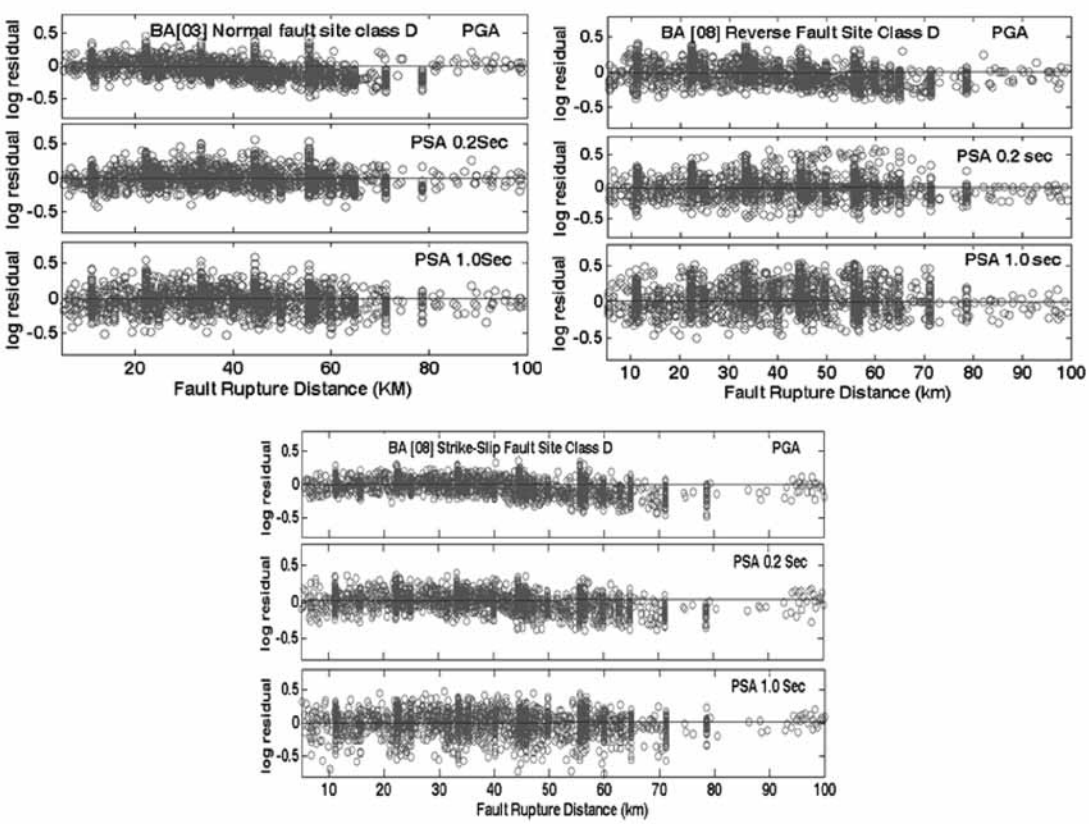

Figure 8. The log residuals with respect to fault-rupture distance for Normal, Reverse and Strike-Slip faulting earthquake mechanisms of the horizontal component of ground motion: PGA and PSA at 0.2 sec and 1.0 sec respectively for Site class D.

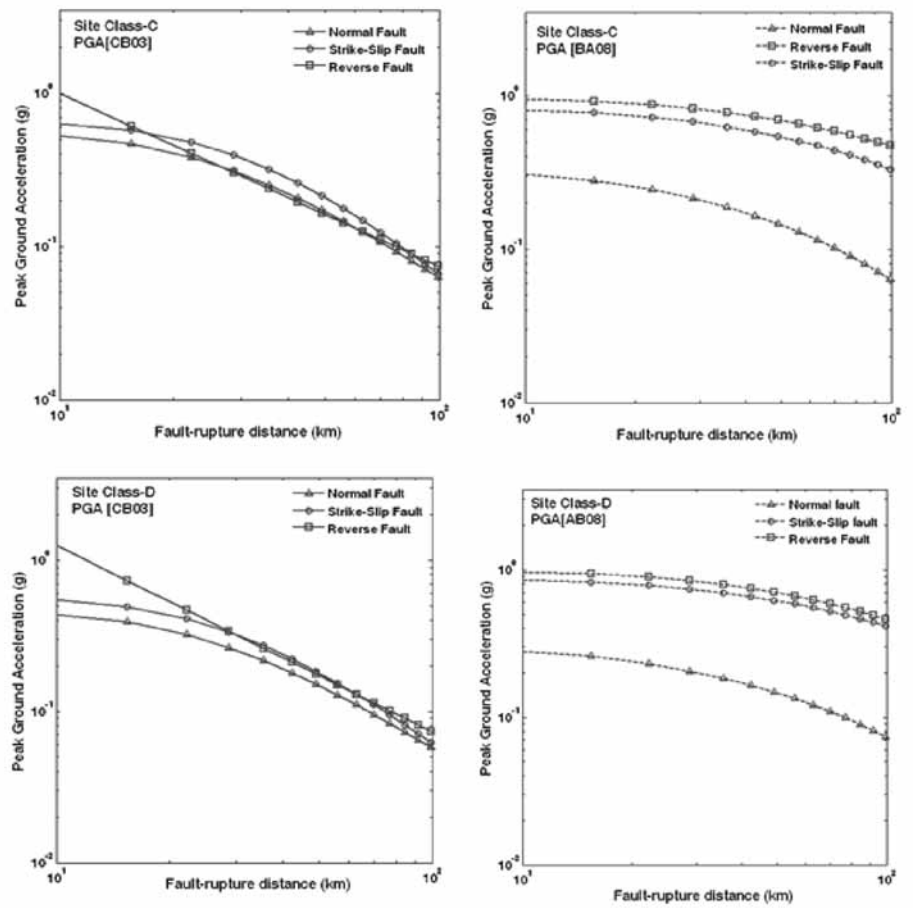

Figure 9. Peak Ground Acceleration estimated for Reverse, Strike-slip and Normal faulting earthquake mechanisms based on Boore and Atkinson (2008), Campbell and Bozorgnia (2003) NGP models for site classes C & D considering Magnitude M_w7.8.

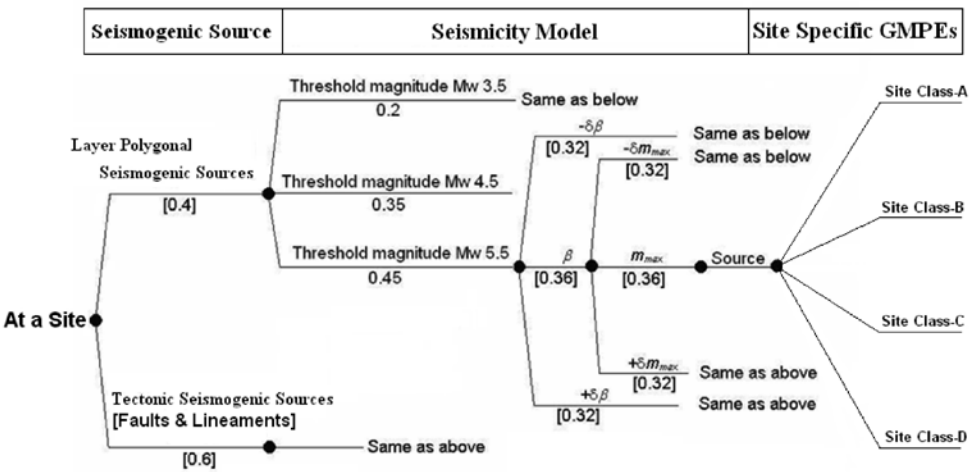

Figure 10. A logic tree formulation for probabilistic seismic hazard computation at each node of the region gridded at 0.005° × 0.005° intervals while the details of site specific GMPEs are given in Figure 6.

earthquake resistant design or seismic safety measures. It is, therefore, important to predict ground-shaking levels in order to determine appropriate building codal provisions for earthquake-resistant design of structures (Silva et al. 2014). The accurate prediction of ground motion for future earthquake scenarios is a key issue in any seismic hazard analysis program. In the present study, the derived NGP models have been utilized for the assessment of surface

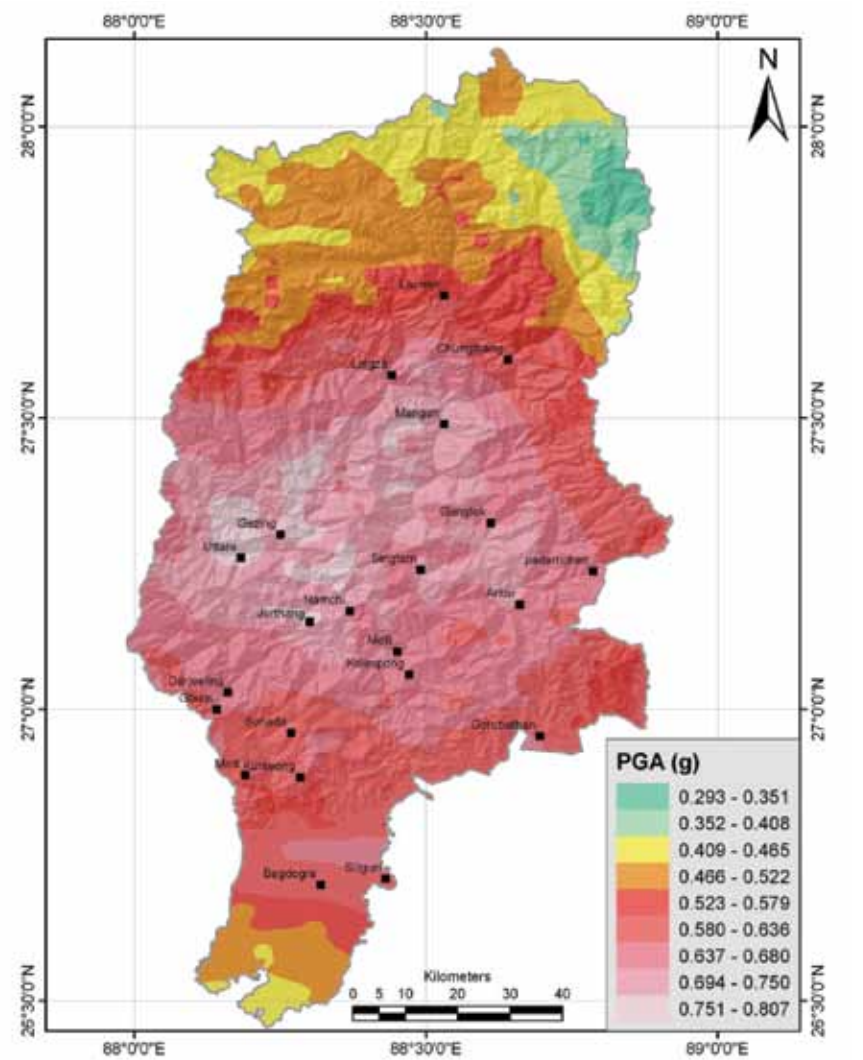

Figure 11. Spatial distribution of PGA with 10% probability of exceedance in 50 years at Surface level in the Darjeeling-Sikkim Himalaya.

consistent probabilistic seismic hazard scenario in this earthquake province for 10% probability of exceedance in 50 years using polygonal seismogenic sources, linear tectonic sources, smoothen gridded seismic activity, seismicity parameters and site specific NGP models incorporating both aleatory and epistemic uncertainties through a logic tree framework as depicted in Figure 10. 41 polygonal seismogenic sources at two hypocentral depth ranges viz. 0-25km and 25-70km have been identified based on seismicity pattern, fault networks & similarity in the style of focal mechanisms. One hundred eighty six major tectonic features (i.e. faults and lineaments) have been identified from the seismotectonic map of India and the additional from Landsat TM/MSS and SRTM data through edge enhancement filtering and principal component analysis in the 0-25 km and 25-70 km depth ranges that have the potential of generating earthquakes of M_w3.5 and above. The evaluation of seismicity parameters is one of the most important steps for hazard estimation. The maximum likelihood method given by Aki (1965) has been used to estimate the b-value. The standard deviation of b-value ($\delta\beta$) has been computed by the bootstrapping method as suggested by Schorlemmer et al. (2003) which involves repeated computations, each time employing different replacement events drawn from the catalog. The maximum earthquake (M_{max}), is the largest seismic event characteristic of the terrain under the tectono-stratigraphic consideration. For polygonal sources a maximum likelihood method for maximum earthquake estimation referred to as Kijko-Sellevoll-Bayesian (Kijko 2004) has been used. The contribution of background seismicity in the hazard perspective is also estimated using smoothen gridded seismicity models given by Frankel (1995) at a regular grid interval of $0.1^o \times 0.1^o$ for the threshold

magnitudes of M_w 3.5, 4.5 and 5.5 respectively at both the hypocentral depth ranges 0-25km and 25-70km as also for each active tectonic source along and its close proximity for the threshold magnitudes of M_w 3.5, 4.5, 5.5 at both the hypocentral depth ranges. The details of seismogenic sources, seismic activity rate and seismicity parameters have been described in Nath and Adhikari (2013). In the present study, 42 site-specific NGP models developed for the three tectonic types' viz. normal, strike-slip and thrust faulting mechanisms of earthquake nucleation as per site classes A, B, C and D for different station elevation ranges have been selected through suitability testing and weighting in a logic tree framework for Probabilistic Seismic Hazard computation. The basic methodology of probabilistic seismic hazard analysis involves computation of ground motion thresholds that are exceeded with a mean return period of say 475 years / 2475 years at a particular site of interest (Cornell 1968, McGuire 1976). The detail methodology of the Probabilistic Seismic Hazard analysis has been discussed in Nath and Thingbaijam (2012), Nath and Adhikari (2013) and Nath et al. (2014). For seismic hazard analysis the entire study region is divided into grid-points at a spacing of $0.005^o \times 0.005^o$ and hazard has been computed at each grid point. Logic tree framework given in Figure 10 has been adopted for the computation of hazard by incorporating multiple models in source considerations, NGPs and seismicity parameters by assigning appropriate weights for source, magnitude and NGPs. The results estimated for each depth range are integrated together and also with the ones obtained for the tectonic sources to establish the overall hazard scenario. For design purpose, 10% probability of exceedance in 50 years has been considered to be more appropriate and is ideally suited. The PGA distribution for 10% probability of exceedance in 50 years at surface level shows a variation from 0.293g to 0.807g for the Darjeeling-Sikkim Himalaya as depicted in Figure 11. The major urban centers like Gangtok, Mangan and Darjeeling exhibits higher hazard to the tune of 0.65g. It is observed that the provision given by BIS (2002) greatly underestimates the urban design posing greater risk to the otherwise seismically vulnerable Himalayan terrain.

CONCLUSIONS

Seismic Hazard is a serious issue in earthquake prone provinces across the globe necessitating an in-depth understanding of the same for earthquake induced disaster mitigation, management and urban safety regulations. 42 next generation prediction models derived in this study for Darjeeling-Sikkim Himalaya can be used along with the other existing GMPEs in the region or in a similar tectonic setup in a logic tree frame work for Probabilistic Seismic Hazard Assessment with defined aleatory uncertainty. Preliminary study on the application of derived NGP models for the probabilistic seismic hazard assessment in Darjeeling Sikkim Himalaya predicts that the major urban centers of Gangtok, Mangan, Singtham, Melli, Jorethang, Uttare and Darjeeling originally placed in Zone IV of BIS Zonation Map of India are associated with enhanced hazard level within a range of 0.60 - 0.750g placing those to higher hazard zones with a predicted zone factor of 0.75g. In addition, the co-efficient estimated for PGA and PSA at 1.0 see and 0.2 sec period can be used in earthquake engineering practices for generating site specific design response spectra for further usage in estimating seismic coefficients for adaptation in the building codal provision as per the BIS guidelines for earthquake safe urbanization.

ACKNOWLEDGEMENTS

This work is supported by the Geoscience Division, Ministry of Earth Sciences, Government of India. The logistic support provided by the Science and Technology Council, Government of Sikkim is thankfully acknowledged. The critical review and constructive suggestions of the anonymous reviewer and the Chief Editor greatly helped in improving the manuscript with enhanced scientific exposition.

REFERENCES

Abrahamson, N. A., and Silva, W. J., 1997. Empirical response spectral attenuation relations for shallow crustal earthquakes, Seismol Res Lett., v.68(1), pp: 94−127.

Acton, C. E., Priestley, K., Mitra, S., and Gaur, V. K., 2011. Crustal structure of the Darjeeling-Sikkim Himalaya and Southern Tibet, Geophys J Int., v.184(2), pp: 829-852.

Aki, K., 1965. Maximum likelihood estimate of b in the formula log N = a - bM and its confidence limits, Bulletin of the Earthquake Research Institute, v.43, pp: 237-239.

Anbazhagan, P., Abhishek, K., and Sitharam, T. G., 2013. Ground motion prediction equation considering combined data set of recorded and simulated ground motions, Soil Dynamics and Earthquake Engineering, v.53, pp: 92–108.

Anderson, J. G., and Hough, S. E., 1984. A model for the shape of the Fourier amplitude spectrum of acceleration at high frequencies, Bull Seismol Soc Am., v.74(5), pp: 1969−1993.

Barazangi, M., and Ni, J., 1982. Velocities and propagation characteristics of P_n and S_n waves beneath the Himalayan Arc and Tibetan Plateau: Possible evidence for under thrusting of Indian continental lithosphere beneath Tibet, Geology, v.10(4), pp:179-185.

BIS, 2002. IS 1893–2002 (Part 1): Indian Standard Criteria for Earthquake Resistant Design of Structures, Part 1–General Provisions and Buildings, Bureau of Indian Standards, New Delhi.

Boore, D. M., and Atkinson, G. M., 2008. Ground-motion prediction equations for the average horizontal component of

PGA, PGV, and 5%-damped PSA at spectral periods between 0.01s and 10.0s., Earthq Spectra, v.24(1), pp: 99–138.

Brune, J. N., 1970. Tectonic stress and the spectra of seismic shear waves from earthquakes, J Geophys Res., v.75(26), pp: 4997–5009.

Brune, J. N., 1968. Seismic Moment, seismicity and rate of slip along major fault zones, J Geophys Res., v.73(2), pp: 777–794.

Campbell, K. W., and Bozorgnia, Y., 2006. Next Generation Attenuation (NGA) empirical ground motion models: Can they be used in Europe? First European Conference on Earthquake Engineering and Seismology, A joint event of the 13th ECEE & 30th General Assembly of the ESC, Geneva, Switzerland.

Campbell, K. W., and Bozorgnia, Y., 2003. Updated near-source ground-motion (attenuation) relations for the horizontal and vertical components of peak ground acceleration and acceleration response spectra, Bull Seismol Soc Am., v.93(1), pp: 314−331.

Castro, R. R., Pacor, F., Sala, A., and Petrungaro, C., 1996. S-wave attenuation and site effects in the region of Friuli, Italy, J Geophys Res., v.101(B10), pp: 22355-22369.

Chopra, S., Sharma, J., Sutar, A., and Bansal, B. K., 2014. Estimation of Source Parameters of M w 6.9 Sikkim Earthquake and Modeling of Ground Motions to Determine Causative Fault, Pure and Applied Geophysics, v.171(7), pp: 1311-1328.

Cornell, C. A., 1968. Engineering seismic risk analysis, Bulletin of Seismological Society of America, v.58, pp: 1583–1606.

Dasgupta, S., Pande, P., Ganguly, D., Iqbal, Z., Sanyal, K., Venaktraman, N.V., Dasgupta, S., Sural, B., Harendranath, L., Mazumdar, K., Sanyal, S., Roy. A., Das, L. K., Misra, P. S., and Gupta, H., 2000. Seismotectonic Atlas of India and its Environs, Geological Survey of India, Calcutta.

De la Torre, T. L., Monsalve, G., Sheehan, A. F., Sapkota, S., and Wu, F., 2007. Earthquake processes of the Himalayan collision zone in eastern Nepal and the southern Tibetan Plateau, Geophysical Journal International, v.171(2), pp: 718-738.

Douglas, J., 2003. Earthquake ground motion estimation using strong-motion records: a review of equations for the estimation of peak ground acceleration and response spectral ordinates, Earth Sci Rev., v.61(1-2), pp: 43-104.

Frankel, A., 1995. Mapping Seismic Hazard in the central and eastern United States. Bulletin of Seismological Society of America, v.66, pp: 8–21.

Gansser, A., 1964. Geology of the Himalayas, Wiley-Interscience Publication, New York.

GSI., 1939. The Bihar-Nepal earthquake of 1934, Mem. Geological Survey of India, v.72, pp: 287-288.

Gupta, H. K., and Singh, D. D., 1980. Spectral analysis of body waves for earthquakes in Nepal Himalaya and vicinity: their focal parameters and tectonic implications, Tectonophysics, v.62(1-2), pp: 53–66.

Joyner, W. B., and Boore, D. M., 1981. Peak Horizontal Acceleration and Velocity from Strong Motion Records Including Records from the 1979 Imperial Valley, California, Earthquake. Bull Seismol Soc Am., v.71 (6), pp: 2011–2038.

Kijko, A., 2004. Estimation of the Maximum Earthquake Magnitude, Pure and Applied Geophysics, v.161, pp: 1655–1681.

Kumar, D., Sarkar, I., Sriram, V., and Khattri, K. N., 2005: Estimation of the source parameters of the Himalaya earthquake of October 19, 1991 average effective shear wave attenuation parameter and local site effects from accelerograms, Tectonophysics, v.407(1-2), pp: 1-24.

McGuire, R. K., 1976. FORTRAN Computer Program for Seismic Risk Analysis, US Geological Survey, Open file report, pp: 76–67.

Mishra, O. P., 2014. Intricacies of the Himalayan seismotectonics and seismogenesis: need for integrated research, Current Science, v.106 (2), pp: 176-187.

Molnar, P., and Chen, W. P., 1983. Focal depths and fault plane solutions of earthquakes under the Tibetan plateau, Journal of Geophysical Research: Solid Earth (1978–2012), v.88(B2), pp: 1180-1196.

Molnar, P., and Lyon-Caent, H., 1989. Fault plane solutions of earthquakes and active tectonics of the Tibetan Plateau and its margins, Geophysical Journal International, v.99(1), pp: 123-153.

Motazedian, D., and Atkinson, G. M., 2005. Stochastic finite-fault modeling based on a dynamic corner frequency, Bull Seismol Soc Am., v.95(3), pp: 995−1010.

Nakata, T., Otsuk, I. K., and Khan, S. H., 1990. Active Faults, stress field and plate motion along Indo Eurasian plate boundary, Tectonophysics, v.181(1-4), pp: 83-95.

Nath, S. K., Raj, A., Thingbaijam, K. K. S., and Kumar, A., 2009. Ground motion synthesis and seismic scenario in Guwahati City - A stochastic approach, Seismol Res Lett., v.80(2), pp: 233−242.

Nath, S. K., and Thingbaijam, K. K. S., 2011. Peak ground motion predictions in India: an appraisal for rock sites, J Seismol., v.15(2), pp: 295-315.

Nath, S. K., Vyas, M., Pal, I., and Sengupta, P., 2005. A Seismic Hazard Scenario in the Sikkim Himalaya from Seismotectonics, Spectral Amplification, Source Parameterization and Spectral Attenuation Laws using Strong Motion Seismometry, J Geophys Res., v.110(B1), pp: 1-20.

Nath, S. K., Thingbaijam, K. K. S., and Raj, A., 2008. Earthquake hazard in the northeast India – A seismic microzonation approach with typical case studies from Sikkim Himalaya and Guwahati city, J. Earth. Sys. Sci., v.117, pp: 809–831.

Nath, S. K., Thingbaijam, K. K. S., 2012. Probabilistic seismic hazard assessment of India, Seismological Research Letter, v.83, pp: 135–149.

Nath, S. K., and Adhikari, M. D., 2013. Next Generation Attenuation Models and Time Independent Probabilistic Seismic Hazard of Darjeeling-Sikkim Himalaya, International

Journal of Earthquake Engineering and Hazard Mitigation, v.1(1), pp: 29-54.

Nath, S. K., Adhikari, M. D., Maiti, S. K., Devaraj, N., Srivastava, N., and Mohapatra, L. D., 2014. Earthquake Scenario in West Bengal with emphasis on Seismic Hazard Microzonation of the city of Kolkata, India, Natural Hazards Earth System Science, v.14, pp: 2549-2575.

Nayak, A., Nath, S. K., Thingbaijam, K. K. S., and Baruah, S., 2011. New insights into path attenuation of ground motions in northeast India and northwest Himalayas, Bull Seismol Soc Am., v.101(5), pp: 2550–2560.

Ordaz, M., and Singh, S. K., 1992. Source spectra and spectral attenuation of seismic waves from Mexican earthquakes, and evidence of amplification in the hill zone of Mexico City, Bull Seismol Soc Am., v.82(1), pp: 24–43.

Pal, I., Nath, S. K., Shukla, K., Pal, D. K., Raj, A., Thingbaijam, K. K. S., and Bansal, B. K., 2008. Earthquake Hazard Zonation of Sikkim Himalaya Using a GIS Platform, Nat Hazards, v. 45(3), pp: 333−377.

Power, M., Chiou, B., Abrahamson, N., Bozorgnia, Y., Shantz, T., Roblee, C., 2008. An overview of the NGA project, Earthq Spectra, v.24(1), pp: 3-21.

Raj, A., Nath, S.K., Bansal, B. K., Thingbaijam, K. K. S., Thiruvengadam, A. N., Yadav, A., and Arrawatia, M. L., 2009. Rapid estimation of source parameters using finite fault modeling-case studies from the Sikkim and Garhwal Himalayas, Seismol. Res. Lett., v.80(1), pp: 89-96.

Saragoni, G. R., and Hart, G. C., 1974. Simulation of Artificial earthquakes, Earthq. Eng. Struct. Dynam., v.2, pp: 249-268.

Sapkota, S. N., Bollinger, L., Klinger, Y., Tapponnier, P., Gaudemer, Y., and Tiwari, D., 2013. Primary surface ruptures of the great Himalayan earthquakes in 1934 and 1255, Nature Geoscience, v.6(1), pp: 71-76.

Schorlemmer, D., Neri, G., Wiemer, S. and Mostaccio, A., 2003. Stability and significance tests for b-value anomalies: Example from the Tyrrhenian Sea, Geophysical Research Letters, 1835, doi: 10.1029/2003GL017335., v.30(16).

Sengupta, P., 2012. Stochastic finite-fault modelling of strong earthquakes in Narmada South Fault, Indian Shield, Journal of Earth System Science, v.121(3), pp: 837-846.

Sharma, M. L., and Wason, H. R., 1994. Occurrence of low stress drop earthquakes in the Garhwal Himalaya region, Phy Earth Planet Int., v.85(3-4), pp: 265–722.

Shoja-Taheri, J., Naserieh, S., and Hadi, G., 2010. A Test of the Applicability of NGA Models to the Strong Ground-Motion Data in the Iranian Plateau, J Earthq Eng., v.14, pp:278–292.

Singh, D. D., Rastogi, B. K., and Gupta, H. K., 1978. Spectral analysis of body waves for earthquakes and their source parameters in the Himalaya and nearby regions, Phy Earth Planet Int., v.18(2), pp: 143–152.

Silva, V., Crowley, H., Varum, H., and Pinho, R., 2014. Seismic risk assessment for mainland Portugal, Bulletin of Earthquake Engineering, v.13 (2), pp: 429-457.

Stafford, P. J., Strasser, F. O., and Bommer, J. J., 2008. An evaluation of the applicability of the NGA models to ground-motion prediction in the Euro-Mediterranean region, Bull Earthq Eng., v.6, pp: 149−177.

Thakur, V. C., Mahajan, A. K., and Gupta, V., 2012. Seismotectonics of September 2011 Sikkim Earthquake: a component of transcurrent deformation in eastern Himalaya, Himalayan Geology, v.33(1), pp: 89-96.

Thingbaijam, K. K. S., and Nath, S. K., 2008. Estimation of maximum earthquakes in northeast India region, Pure Appl Geophys, v.165(5), pp: 889−901.

Thiruvengadam, N., 2009. Deterministic Seismic Hazard Scenario of North-East India through Stochastic Ground Motion Simulation and Site Depended Attenuation Models, M. Tech. dissertation, Dept. Geology and Geophysics, Indian Institute of Technology, Kharagpur, India.

Wells, D. L., and Coppersmith, K. J., 1994. New empirical relations among magnitude rupture length, rupture width, rupture area, and surface displacement, Bull Seismol Soc Am, v.84(4), pp: 974−1002.